Quasiparticle–phonon model of the nucleus II. The phonon space and giant $E\lambda$ resonances in deformed nuclei

L. A. Malov and V. G. Solov'ev

Joint Institute for Nuclear Research, Dubna

Fiz. Elem. Chastits At. Yadra **11**, 301–341 (March–April 1980)

The results are given of calculations of singlephonon states in even–even deformed nuclei, which form a basis in the quasiparticle–phonon model of the nucleus. It is shown that the calculations of the singlephonon states with multipolarity $\lambda = 1, 2$, and 3 have a unique result, while those with multipolarity $\lambda \geq 4$ contain a certain arbitrariness associated with the choice of the constants of the multipole–multipole interactions. The parameters of the calculations in deformed nuclei in the regions $150 \leq A \leq 190$ and $226 \leq A < 260$ are systematized. In the singlephonon approximation, a fairly good description is obtained of the positions and widths of giant dipole, quadrupole, and octupole resonances. The results of calculations of $E\lambda$ resonances of high multipolarity are given.

PACS numbers: 21.60.Gx

INTRODUCTION

In the framework of the quasiparticle-phonon model of the nucleus one can calculate the few-quasiparticle components of the wave functions of nuclear states at low, intermediate, and high excitation energies. The quasiparticle-phonon model of the nucleus is a generalization of the models of Ref. 1, which describe low-lying states, to a wide range of excitation energies. The possibility of a unified description of a number of characteristics of medium and heavy nuclei in a wide range of excitation energies was indicated in Refs. 2–4. In recent years, the series of studies of Refs. 5–21 have shown how this program is implemented in practice. These have included calculations of the characteristics of excited states that are determined by the fragmentation of the single-quasiparticle and single-phonon states over the nuclear levels.

The main features of the quasiparticle-phonon model of the nucleus were set forth in Ref. 22. A great advantage of the model derives from its use of single-phonon states, and not of single-particle states, as its basis. This means that the basis itself takes into account simultaneously collective vibrational, weakly collective, and two-quasiparticle states. The calculations in Ref. 23 of the density of nuclear states indicate that the phonon space is complete.

The calculation of the phonon space is a first and important step in the calculations in the quasiparticle-phonon model of the nucleus. In deformed nuclei (in contrast to spherical nuclei), a complete phonon basis can be constructed only by means of multipole phonons. This is due to the fact that for each multipolarity λ there are phonons with projection of K onto the symmetry axis of the nucleus equal to $0, 1, 2, \ldots, \lambda$. Therefore, one can form phonons with all spins and parities up to $K = K_{\max}$ by taking multipole forces with $\lambda = 1, 2, 3, \ldots, K_{\max}$. Thus, the multipole phonons form a complete phonon space and there is no need to introduce spin-multipole phonons. This is true if one is not specially interested in magnetic transitions. It is known that there are collective spin-multipole states for which the probabilities of $M\lambda$ transitions are fairly high. However, the multipole phonons, especially at not large energies, are more strongly collectivized than the spin-multipole phonons with the same values of K^{π}. Therefore, the phonon basis is constructed solely from multipole phonons. The spin-multipole phonons are used to study the magnetic moments, $M\lambda$ transitions between nuclear states, and giant magnetic resonances.

In the present paper, we give the results of calculations of the phonon basis for deformed nuclei. The numerical calculations are restricted to the regions $150 \leq A \leq 190$ and $226 \leq A < 260$. The investigations have shown that in deformed nuclei in the single-phonon approximation a fairly good description of the energies and widths of giant resonances can be obtained. The results of the calculations of giant multipole resonances in deformed nuclei are summarized. In the present review, we use the formulas given in Ref. 22 and, as a rule, the same notation.

1. AVERAGE FIELD AND PARAMETERS OF THE CALCULATIONS

In the quasiparticle-phonon model of the nucleus, the Hamiltonian consists of the Woods–Saxon potential, which describes the average field of the neutron and proton systems, and interactions leading to pairing correlations of superconducting type, multipole-multipole interactions, and spin-multipole-spin-multipole interactions, which are here ignored. In accordance with Ref. 22, the Hamiltonian of the model has the form

$$H_M = H_P + H_Q. \tag{1}$$

The energies and wave functions of the single-phonon states are calculated on the basis of the single-particle energies and wave functions of the axisymmetric Woods–Saxon potential. The shape of the nucleus is described by

$$R(\theta) = R_0\{1 + \beta_0 + \beta_2 Y_{20}(\theta) + \beta_4 Y_{40}(\theta)\}, \tag{2}$$

where $R_0 = r_0 A^{1/3}$ is the radius of an equally large spherical nucleus, β_0 is a constant introduced to ensure better fulfillment of the condition of conservation of the volume of the nucleus, and β_2 and β_4 are the parameters of the quadrupole ($\lambda = 2$) and hexadecapole ($\lambda = 4$) deformations. The nuclear part of the Woods–Saxon

 0090-4759/80/020111-15$02.80

potential consists of two parts:

$$V_{\text{nucl}}(\mathbf{r}) = V(r) + V_{ls}(\mathbf{r}); \quad (3)$$

$$V(r) = -V_0/\{1+\exp[\alpha(r-R(\theta))]\}; \quad (4)$$

$$V_{ls}(\mathbf{r}) = -\varkappa(\mathbf{p}\times\sigma)\nabla V(r), \quad (5)$$

where σ are the Pauli matrices and p is the nucleon momentum. For the proton system, it is necessary to add the Coulomb term

$$V_c(\mathbf{r}) = \frac{3}{4\pi}\frac{(Z-1)e^2}{R_0^3} \times \int \frac{dr'}{|\mathbf{r}-r'|}\{1+\exp[\alpha(r'-R(\theta))]\}^{-1}. \quad (6)$$

The energy eigenvalues and the wave functions for the Woods–Saxon potential can be calculated approximately by an expansion in a spherical basis.[14]

The energies and wave functions of single-particle states, which are solutions of the Schrödinger equation with the Woods–Saxon potential, depend on the mass number A. Therefore, in the calculations the deformed nuclei are distributed over A zones. These zones are given in Table I. For each zone, the parameters β_2^0 and β_4^0 of the equilibrium deformation and the constants of the interactions are fixed. For the correct description of the single-quasiparticle levels in nuclei with an odd number of neutrons and in nuclei with an odd number of protons the parameters of the potential are fitted. This fitting consists of four stages: 1) The single-particle energies and wave functions are calculated with one set of parameters $V_0, r_0, \alpha, \varkappa$; 2) the shell-correction method[25] is used to find the equilibrium shape of the nucleus, this fixing the parameters β_2^0, β_4^0; 3) the phonons are calculated; 4) the interactions of the quasiparticles with the phonons are taken into account and the energies and wave functions of the nonrotational states of odd nuclei are calculated and compared with the corresponding experimental data. If necessary, the parameters of the Woods–Saxon potential are then modified and the four stages in the calculations are repeated. The procedure is continued until a sufficiently good description of the experimental data for the nonrotational levels of odd nuclei has been obtained.

The parameters of the Woods–Saxon potential are given in Table I. It can be seen that there is a small change in the parameters on the transition from one zone to the next. The small fluctuations of the parameters are due to the fact that the representation of the average field by the Woods–Saxon potential is fairly good but not perfect. The comparatively simple form of the potential can often be effectively compensated by small changes of the parameters. We note that the parameters of the spherically symmetric Woods–Saxon potential used to describe spherical nuclei in the zones with $A = 59$, 91, 121, 141, and 209 and given in Ref. 21 differ little from the parameters given in Table I.

TABLE I. Parameters of the nonspherical Woods—Saxon potential.

A band	Neutron system				Proton system			
	V_0, MeV	r_0, F	α, F^{-1}	F^2	V_0, MeV	r_0, F	α, F^{-1}	$\varkappa, F^2$
155	47.2	1.26	1.67	0.40	59.2	1.24	1.69	0.36
165	44.8	1.26	1.67	0.43	59.2	1.25	1.63	0.355
173	44.8	1.26	1.67	0.42	59.2	1.25	1.59	0.32
181	43.4	1.26	1.67	0.40	59.8	1.24	1.67	0.33
229	47.0	1.26	1.40	0.47	60.5	1.24	1.55	0.375
239	46.7	1.26	1.45	0.43	61.0	1.24	1.55	0.375
247	46.0	1.26	1.38	0.43	62.0	1.24	1.55	0.370
255	46.0	1.26	1.30	0.47	62.5	1.24	1.55	0.360

The single-particle energies and wave functions of the Woods–Saxon potential for nuclei in the region $150 \leqslant A \leqslant 190$ are given in Ref. 26, and those in the region $226 \leqslant A < 260$ are given partly in Ref. 27.

Because of the large quadrupole deformation, there is fragmentation (distribution of the strength) of the subshells of the spherically symmetric Woods–Saxon potential over several single-particle levels of the axisymmetric Woods–Saxon potential. This fragmentation is large, which is shown in Fig. 1 for the subshell $3p_{1/2}$ in the neutron system with $A = 155$.

The calculations take into account the greatest possible number of single-particle levels. The numbers of single-particle neutron (n_N) and proton (n_Z) levels for each A zone and the parameters of the equilibrium deformations are given in Table II. The constants G_N and G_Z of the pairing correlations of superconducting type were determined from the experimental data on the pairing energies. The values of $G_N A$ and $G_Z A$ are given in Table II, which shows that these quantities remain virtually constant as A varies from 150 to 260.

The form of the isoscalar and isovector multipole–multipole interactions is given in Ref. 22. The isoscalar $\varkappa_0^{(\lambda\mu)}$ and isovector $\varkappa_1^{(\lambda\mu)}$ constants are determined as follows:

1) the isovector constants $\varkappa_1^{(10)}$ and $\varkappa_1^{(11)}$ from the position of the giant $E1$ resonance. To eliminate a ghost state, one introduces isoscalar dipole forces with a constant $\varkappa_0^{(1\mu)}$, which leads to the vanishing of the first root of the corresponding secular equation;

2) the isoscalar constants $\varkappa_0^{(2\mu)}$ and $\varkappa_0^{(3\mu)}$ from the energies of the first quadrupole and octupole states, and the ratios $\varkappa_1^{(\lambda\mu)}/\varkappa_0^{(\lambda\mu)}$ from the position of the corresponding isovector resonance;

3) for $\lambda \geqslant 4$, the estimates[28]

$$\varkappa_0^{(\lambda)} = \frac{4\pi}{2\lambda+1}\frac{m\omega_0^2}{A\langle r^{2\lambda-2}\rangle}; \quad (7)$$

$$\varkappa_1^{(\lambda)} = -\pi V/(A\langle r^{2\lambda}\rangle), \quad (8)$$

where $V = 120$ MeV, are used. Somewhat smaller values of these constants are taken to prevent the corresponding first states from sinking and being too strongly collectivized.

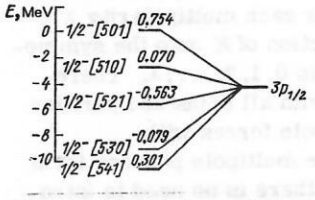

FIG. 1. Distribution of the strength of the $3p_{1/2}$ subshell over the single-particle states with $K^\pi = \frac{1}{2}^-$ in the neutron system with $A = 155$ at $\beta_2 = 0.27$ and $\beta_4 = 0.04$. The numbers above the levels indicate the values of the components in the expansion of the wave function of the deformed Woods—Saxon potential in a spherical basis.

TABLE II. Parameters used in the calculation of the energies and wave functions of single-phonon states.

A band	Number of single-particle levels n_N	n_Z	Deformation parameters β_2^0	β_4^0	Pairing constants $G_Z A$, MeV	$G_Z A$, MeV	Constants of the multipole-multipole interaction: $\lambda=1$, $\varkappa_1/\varkappa_0=-1,2$ $\varkappa_0^{(10)} A^{5/3}$	$\varkappa_0^{(11)} A^{5/3}$	$\lambda=2$, $\varkappa_1/\varkappa_0=-1,5$ $\varkappa_0^{(20)} A^{7/3}$	$\varkappa_0^{(21)} A^{7/3}$	$\varkappa_0^{(22)} A^{7/3}$	$\lambda=3$, $\varkappa_1/\varkappa_0=-1,5$ $\varkappa_0^{(30)} A^3$	$\varkappa_0^{(31)} A^3$	$\varkappa_0^{(32)} A^3$	$\varkappa_0^{(33)} A^3$
155	104	115	0.30	0.04	18.3	22.6	228	270	219	187	259	138	130	156	216
165	104	132	0.28	0.02	18.7	21.8	223	260	216	172	251	126	126	137	144
173	104	135	0.26	−0.02	18.7	21.7	231	265	208	167	267	131	129	137	142
181	104	135	0.24	−0.03	19.0	21.9	237	270	204	182	250	—	—	—	—
229	150	171	0.19	0.10	17.2	21.4	223	250	208	208	247	130	132	157	—
239	155	175	0.22	0.08	17.2	21.0	220	250	220	202	266	133	135	157	150
247	159	185	0.23	0.06	17.8	21.3	—	—	222	184	268	128	128	155	148

In Table II we give the values of $\varkappa_0^{(\lambda\mu)} A^{(2\lambda+3)/3}$ and the ratio $\varkappa_1^{(\lambda\mu)}/\varkappa_0^{(\lambda\mu)}$ for $\lambda=1$, 2, and 3. It can be seen from Table II that the constants $\varkappa_0^{(\lambda\mu)} A^{(2\lambda+3)/3}$ vary little in a wide range of nuclei with A from 155 to 260. The small change in the constants on the transition from one A zone to another indicates a fairly good description in the single-phonon approximation of the collective vibrational states.

2. SINGLE-PHONON STATES

We give formulas for the single-phonon states generated by multipole-multipole forces in the particle-hole channel.

The part of the model Hamiltonian H_v without the terms needed to describe the 0^+ states has the form

$$H_v = \sum_q \varepsilon(q) B(qq) - \frac{1}{2} \sum_{\lambda\mu i i'} \Big\{ (\varkappa_0^{(\lambda\mu)} + \varkappa_1^{(\lambda\mu)}) \times \Big[\sum_{\substack{ss', \\ s_2 s_2}} u_{ss}^{(+)} u_{s_2 s_2'}^{(+)} f^{\lambda\mu}(ss') g_{ss'}^{\lambda\mu i} f^{\lambda\mu}(s_2 s_2') g_{s_2 s_2'}^{\lambda\mu i'} + \sum_{\substack{rr', \\ r_2 r_2'}} u_{rr'}^{(+)} u_{r_2 r_2'}^{(+)} f^{\lambda\mu}(rr') g_{rr'}^{\lambda\mu i} f^{\lambda\mu}(r_2 r_2') g_{r_2 r_2'}^{\lambda\mu i'} \Big] - (\varkappa_0^{(\lambda\mu)} - \varkappa_1^{(\lambda\mu)}) \sum_{\substack{ss', \\ rr'}} u_{ss}^{(+)} u_{rr}^{(+)} [f^{\lambda\mu}(ss') g_{ss'}^{\lambda\mu i} f^{\lambda\mu}(rr') g_{rr'}^{\lambda\mu i'} + f^{\lambda\mu}(ss') g_{ss'}^{\lambda\mu i'} f^{\lambda\mu}(rr') g_{rr'}^{\lambda\mu i}] \Big\} Q_{\lambda\mu i}^{+} Q_{\lambda\mu i'}. \quad (9)$$

The phonon operator has the form

$$Q_t^{+} = \frac{1}{2} \sum_{qq'} \{ \psi_{qq'}^t A^{+}(qq') - \varphi_{qq'}^t A(qq') \}, \quad (10)$$

where $\lambda\mu i \equiv t$, $g_{qq'}^t = \psi_{qq'}^t + \varphi_{qq'}^t$; $w_{qq'}^t = \psi_{qq'}^t - \varphi_{qq'}^t$, and the remaining notation is given in Ref. 22.

The secular equation determining the energies of the single-phonon states ω_t and taking into account the isoscalar and isovector multipole forces with constants $\varkappa_0^{(\lambda\mu)}$, $\varkappa_1^{(\lambda\mu)}$ has the form

$$\mathcal{F}(\omega_t) = -(\varkappa_0^{(\lambda\mu)} + \varkappa_1^{(\lambda\mu)})(X^t(n) + X^t(p)) + 4\varkappa_0^{(\lambda\mu)} \varkappa_1^{(\lambda\mu)} X^t(n) X^t(p) + 1 = 0, \quad (11)$$

where

$$X^t(n) = 2 \sum_{ss'} \frac{f^t(ss') \tilde{f}^t(ss') (u_{ss'}^{(+)})^2 \varepsilon(ss')}{\varepsilon^2(ss') - \omega_t^2}; \quad (12)$$

$f^t(ss')$ is the matrix element of the multipole operator, i is the number of the root of Eq. (11), and $\varepsilon(ss')$ are the energies of the two-quasiparticle states. The remaining notation is given in Ref. 22.

In the quasiparticle-phonon model of the nucleus, all roots of the corresponding secular equation up to energies 30 MeV and higher are calculated for each value of K^π. For each value of K^π, several hundred roots and wave functions are calculated. The following rules are used in these calculations:

1) multipole forces are used to calculate single-phonon states with $K^\pi = 0^\pm, 1^\pm, \ldots, 6^\pm, 7^-$;

2) for each value of K^π, the secular equations with forces of minimal multipolarity are solved;

3) the interactions in the particle-hole channel are taken into account; the interaction in the particle-particle channel is taken into account in the calculation of the single-phonon 0^+ states;

4) in the calculation of the $B(E\lambda)$ values, all states with $I=\lambda$ and $K=0, 1, \ldots, \lambda$ are taken into account.

The first states with $K^\pi = 0^+$ and 2^+ are collective, and for them the $B(E2)$ values are between two and eight single-particle units. The largest two-quasiparticle component reaches 10–50% in the normalization of the wave function. The contribution of the three largest components exceeds 50–70%. In the majority of cases, the first octupole states with $K^\pi = 0^-$, 1^-, and 2^- are collective. The values of the six largest two-quasiparticle components for the first single-phonon states are given for nuclei in the region $150 \leqslant A \leqslant 190$ in Ref. 29 and in the region $228 \leqslant A \leqslant 260$ in Ref. 30.

In turn, the strength of the two-quasiparticle states is distributed over a large number of single-phonon states. Table III shows how the strength of a number of two-quasiparticle neutron states in ^{238}U is distributed over the single-phonon states.

3. STRENGTH FUNCTIONS FOR γ TRANSITIONS

We write down here formulas for the reduced probabilities of γ transitions from the ground states of even-even nuclei to excited states with $I_f^{\pi_f} K_f$. When the multipolarity of the electric transition is equal to the multipolarity of the phonon of the excited state, we have in accordance with Ref. 1

$$B(E\lambda;\ 0^+0 \to I_f^{\pi_f} K_f) = (00\lambda\mu \mid I_f K_f)^2 \mathcal{M}^2; \quad (13)$$

$$\mathcal{M} = \Big(\frac{2-\delta_{\mu 0}}{2}\Big)^{1/2} \Big\{ e_{\text{eff}}^{(\lambda)}(p) \sum_{rr'} f^{\lambda\mu}(rr') g_{rr'}^t u_{rr'}^{(+)} + e_{\text{eff}}^{(\lambda)}(n) \sum_{ss'} f^{\lambda\mu}(ss') g_{ss'}^t u_{ss'}^{(+)} \Big\}. \quad (14)$$

TABLE III. Distribution of the strength of two-quasiparticle neutron states over the single-phonon $K^\pi = 2^+$ states in ^{238}U.

ss'	Components, %: $i=1$	4	7	8	9	10	12	13	16	17	18
	ω_{22^+} (MeV) = 1.06	2.10	2.46	2.49	2.54	2.55	2.66	2.72	2.85	2.87	3.04
633↓— 631↓	20.6	75.6	1.3	0.1	—	—	—	—	—	—	—
622↑— 620↑	9.6	2.0	0.3	0.2	0.3	0.3	8.5	10.7	38.4	12.4	4.8
631↑+ 631↓	8.0	3.5	7.9	18.8	31.6	13.6	8.6	3.0	—	—	—
734↑— 752↑	7.2	2.7	2.0	2.1	14.6	37.0	23.0	4.2	—	—	—

The effective electric charges are equal to

$$e^{(\lambda)}_{\text{eff}}(p)=e+e^{(\lambda)}_{\text{pol}}(p);\quad e^{(\lambda)}_{\text{eff}}(n)=e^{(\lambda)}_{\text{pol}}(n), \tag{15}$$

where, in accordance with Ref. 31,

$$e^{(\lambda)}_{\text{pol}}(p)=e^{(\lambda)}_{\text{pol}}(T=0)-e^{(\lambda)}_{\text{pol}}(T=1);\quad e^{(\lambda)}_{\text{pol}}(n)$$
$$=e^{(\lambda)}_{\text{pol}}(T=0)+e^{(\lambda)}_{\text{pol}}(T=1).$$

For $E1$ transitions, the effective charges are

$$e^{(1)}_{\text{eff}}(p)=(N/A)\,e;\quad e^{(1)}_{\text{eff}}(n)=-(Z/A)\,e. \tag{16}$$

We use Eqs. (11) and (12) and also Eqs. (59), (61), (63), and (64) in Ref. 22, and obtain

$$\mathscr{M}=\frac{1}{2}\left(\frac{2-\delta_{\mu 0}}{Y_t}\right)^{1/2}[e^{(\lambda)}_{\text{eff}}(p)\,X^t(p)\,y^t_p+e^{(\lambda)}_{\text{eff}}(n)\,X^t(n)] \tag{17}$$

and further

$$\mathscr{M}^2=\frac{2-\delta_{\mu 0}}{\partial\mathscr{F}(\omega)/\partial\omega}\{(e^{(\lambda)}_{\text{eff}}(p))^2X^t(p)[1-(\varkappa_0^{(\lambda\mu)}+\varkappa_1^{(\lambda\mu)})X^t(n)]$$
$$+(e^{(\lambda)}_{\text{eff}}(n))^2X^t(n)[1-(\varkappa_0^{(\lambda\mu)}+\varkappa_1^{(\lambda\mu)})X^t(p)]$$
$$+2e^{(\lambda)}_{\text{eff}}(n)\,e^{(\lambda)}_{\text{eff}}(p)(\varkappa_0^{(\lambda\mu)}-\varkappa_1^{(\lambda\mu)})X^t(n)\,X^t(p)\}. \tag{18}$$

As a result, we find the reduced probability of the $E\lambda$ transition in the form

$$B(E\lambda;\ 0^+0\to I_f^\pi K_f)\equiv B(E\lambda;\ 0\to\omega_t)$$
$$=(00\lambda\mu\mid I_fK_f)^2\frac{2-\delta_{\mu 0}}{\partial\mathscr{F}(\omega_t)/\partial\omega_t}\{(e^{(\lambda)}_{\text{eff}}(p))^2X^t(p)$$
$$+(e^{(\lambda)}_{\text{eff}}(n))^2X^t(n)-[\varkappa_0^{(\lambda\mu)}(e^{(\lambda)}_{\text{eff}}(p)-e^{(\lambda)}_{\text{eff}}(n))^2$$
$$+\varkappa_1^{(\lambda\mu)}(e^{(\lambda)}_{\text{eff}}(p)+e^{(\lambda)}_{\text{eff}}(n))^2]X^t(n)\,X^t(p)\}\equiv\frac{P(\omega_t)}{\partial\mathscr{F}(\omega_t)/\partial\omega_t}. \tag{19}$$

To study γ transitions to states of intermediate or high excitation energy, the strength functions for the reduced probabilities of γ transitions are used. We define the strength function $b(E\lambda,\omega)$ as follows:

$$b(E\lambda,\omega)=\sum_t B(E\lambda;\ 0\to\omega_t)\,\rho(\omega-\omega_t). \tag{20}$$

We choose the weight function $\rho(\omega-\omega_t)$ in the form

$$\rho(\omega-\omega_t)=\frac{1}{2\pi}\frac{\Delta}{(\omega-\omega_t)^2+(\Delta/2)^2}. \tag{21}$$

This function has a maximum at $\omega=\omega_t$ and decreases rapidly, approaching zero as $|\omega-\omega_t|\to\infty$, and it is normalized as follows:

$$\int_{-\infty}^{\infty}\rho(\omega-\omega_t)\,d\omega=1.$$

In (20), the summation is over the complete set of states t with a given value of K^π. However, because of the rapid decrease of the function (21) with increasing distance of ω from ω_t,

$$\int_{\omega-\Delta/2}^{\omega+\Delta/2}b(E\lambda,\omega')\,d\omega'\approx\sum_{t\,\Delta}B(E\lambda;\ 0\to\omega_t). \tag{22}$$

The strength function (20) can be written in the form of the contour integral

$$b(E\lambda,\omega)=\frac{\Delta}{2\pi}\sum_t\frac{P(\omega_t)}{\partial\mathscr{F}(\omega_t)\,\partial\omega_t}\frac{1}{(\omega-\omega_t)^2+(\Delta/2)^2}$$
$$=\frac{\Delta}{2\pi}\frac{1}{2\pi i}\int_{C_t}\frac{P(z)}{\mathscr{F}(z)}\frac{dz}{(\omega-z)^2+(\Delta/2)^2}, \tag{23}$$

where the contour of integration C_t is shown in Fig. 2. Equation (23) is obvious, since the function $t(z)=P(z)\rho(\omega-z)/\mathscr{F}(z)$ has simple poles at the points $z=\omega_t$. Bearing in mind that the function $t(z)$ is meromorphic and, therefore, that the sum of the residues of all its

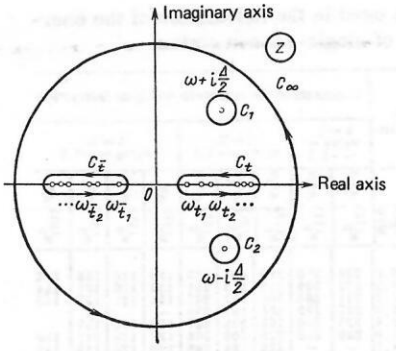

FIG. 2. Contour of integration in the complex z plane.

singularities, including the point at infinity, is zero, we can represent $b(E\lambda,\omega)$ in the form

$$b(E\lambda,\omega)\equiv\oint_{C_t}=-\oint_{C_\infty}-\oint_{C_{\bar t}}-\oint_{C_1+C_2}. \tag{24}$$

We have here used the holomorphicity of the integrand $t(z)$ at the points $z=\pm\varepsilon(qq')$. The integral around the contour C_∞ vanishes, since at large z the integrand is proportional to z^{-4}. The strength function $b(E\lambda,\omega)$ has physical meaning only for $\omega>0$, and it is readily seen that

$$\oint_{C_{\bar t}}=\frac{\Delta}{2\pi}\sum_t\frac{P(\omega_t)}{\partial\mathscr{F}(\omega_t)/\partial\omega_t}\frac{1}{(\omega+\omega_t)^2+(\Delta/2)^2}, \tag{25}$$

i.e., it decreases monotonically as $\sim\omega^{-2}$, and for sufficiently large values of ω it can be ignored. The largest contribution will be made by (25) in the calculation of the reduced probability for the lowest states, but in this case the number of levels is small and the exact expression (19) can be used. Direct calculations confirm that the contribution of (25) to (24) is negligibly small even when ω is equal to the energy of the lowest phonon; it is less than 1%. We calculate the contour integral $\int_{C_1+C_2}$ around the points $z_{1,2}=\omega\pm i\Delta/2$, which are poles of the function $\rho(\omega-z)$, and we obtain

$$b(E\lambda,\omega)\cong-\oint_{C_1+C_2}=\frac{\Delta}{2\pi}\sum_{1,2}\operatorname{res}\left[\frac{P(z)}{\mathscr{F}(z)}\frac{1}{(\omega-z)^2+(\Delta/2)^2}\right]_{z_{1,2}=\omega\pm i\Delta/2}$$
$$=\frac{1}{\pi}(00\lambda\mu\mid I_fK_f)^2(2-\delta_{\mu 0})\operatorname{Im}\left\{\frac{P(\omega)}{\mathscr{F}(\omega)}\right\}_{\omega\to\omega+i\Delta/2}. \tag{26}$$

Sum rules of a different type are helpful for studying giant multipole resonances. They enable one to estimate the extent to which the giant resonances are collective. It can be shown that if the operator of the $E\lambda$ transition is represented in the form

$$\hat Q=\sum_t\mathscr{M}(Q_t+Q_t^+), \tag{27}$$

where Q_t^+ and $\mathscr{M}$ are determined by the expressions (10) and (14), then

$$S_\lambda=\sum_t\omega_tB(E\lambda;\ 0\to\omega_t)=\frac{1}{2}\langle[\hat Q,[H_v,\hat Q]]\rangle$$
$$=e^2(2-\delta_{\mu 0})\Big\{(e^{(\lambda)}_{\text{eff}}(p))^2\sum_{rr'}(u^{(+)}_{rr'}f^{\lambda\mu}(rr'))^2\varepsilon(rr')$$
$$+(e^{(\lambda)}_{\text{eff}}(n))^2\sum_{ss'}(u^{(+)}_{ss'}f^{\lambda\mu}(ss'))^2\varepsilon(ss')\Big\}. \tag{28}$$

This is a model-dependent energy-weighted sum rule (EWSR). It enables one to determine the fraction of the strength of $E\lambda$ transitions for states lying in a definite range of excitation energy.

Of particular interest is the so-called *model-independent energy-weighted sum rule*. If we neglect exchange and velocity-dependent forces in the summation over the excited levels lying below the threshold of meson production, we obtain the following sum rule for $\lambda>1$, $T=0, 1$ (see, for example, Ref. 32):

$$S_\lambda=\sum_t \omega_t B(E\lambda;\ 0\to\omega_t)=3\frac{\lambda(2\lambda+1)}{4\pi}\frac{Ze^2\hbar^2}{2m}R_0^{2\lambda-2}$$
$$=4.8\lambda(3+\lambda)^2 ZA^{-2/3}B_{SP}(E\lambda),\ \text{MeV}, \qquad (29)$$

where $R_0=r_0A^{1/3}$, $r_0=1.2$ F, and

$$B_{SP}(E\lambda)=\frac{2\lambda+1}{4\pi}\left(\frac{3}{3+\lambda}\right)^2 R_0^{2\lambda}e^2$$

is the single-particle probability of the $E\lambda$ transition. We here sum transitions to single-phonon states with all possible values of μ for given λ. For example, for $\lambda=2$ the left-hand sides of (28) and (29) contain transitions to states with $I_f^{\pi_f}K_f$ equal to 2^+0, 2^+1, and 2^+2.

In the case of the $E1$ transition, the EWSR has the form

$$S_1=\sum_t \omega_t B(E1;\ 0\to\omega_t)=\frac{9}{8\pi}\frac{e^2\hbar^2}{m}\frac{NZ}{A}, \qquad (30)$$

which goes over into the well-known Thomas-Reich-Kuhn sum rule for the cross section of dipole photoabsorption,

$$\sigma_{E1}=\int_0^\infty \sigma_{E1}(\omega)\,d\omega=\sum_g \sigma_{E1}(\omega_g)$$
$$=\frac{2\pi^2e^2\hbar}{mc}\frac{NZ}{A}=60\frac{NZ}{A},\ \text{MeV}\cdot\text{mb} \qquad (31)$$

if we use the relation between the cross section of photoabsorption at level t and the probability of the electric transition $0\to\omega_t$:

$$\sigma_{E\lambda}(\omega_t)=\pi^2\left(\frac{\hbar c}{\omega_t}\right)^2\hbar w(E\lambda;\ 0\to\omega_t); \qquad (32)$$

$$w(E\lambda;\ 0\to\omega_t)=8\pi\frac{\lambda+1}{\lambda[(2\lambda+1)!!]^2}\left(\frac{\omega}{\hbar c}\right)^{2\lambda+1}B(E\lambda;\ 0\to\omega_t). \qquad (33)$$

In some cases, the relations between the cross sections of photoabsorption and the probabilities of the corresponding electric transitions for the lowest multipolarities may be helpful:

$$\sigma_{E\lambda}(\omega_t)=\begin{cases}0.282\omega_tB(E1;\ 0\to\omega_t)\ [e^2\cdot F]=\\ =4.04\omega_tB(E1;\ 0\to\omega_t)\ [\text{MeV}\cdot\text{mb}];\\ 0.217\cdot10^{-6}\omega_t^3B(E2;\ 0\to\omega_t)\ [e^2\cdot F]=\\ =3.12\cdot10^{-6}\omega_t^3B(E2;\ 0\to\omega_t)\ [\text{MeV}\cdot\text{mb}];\\ 0.101\cdot10^{-12}\omega_t^5B(E3;\ 0\to\omega_t)\ [e^2\cdot F]=\\ =1.44\cdot10^{-12}\omega_t^5B(E3;\ 0\to\omega_t)\ [\text{MeV}\cdot\text{mb}].\end{cases} \qquad (34)$$

In addition, for the giant electric dipole resonance one usually uses the moments of the photoabsorption cross section ($n=-1, -2$):

$$\sigma_n=\frac{16\pi^3}{9}\sum_t \omega_t^{n+1}B(E1;\ 0\to\omega_t). \qquad (35)$$

The method of strength functions can be used to find energy-weighted sums S_λ and the photoabsorption cross sections $\sigma_{E\lambda}$, σ_{-1}, and σ_{-2}. Carrying out the same procedure as in the derivation of Eq. (26) for the energy-weighted sum, we obtain

$$S_\lambda(\omega)=\sum_t \omega_tB(E_\lambda;\ 0\to\omega_t)\rho(\omega-\omega_t)=\frac{1}{\pi}\operatorname{Im}\frac{zP(z)}{\mathcal{F}(z)}\Big|_{z=\omega+i\Delta/2}. \qquad (36)$$

The method of strength functions has a considerable practical advantage over the traditional method, which requires a computer solution of a very large number of complicated equations for the direct determination of the energies and wave functions of excited states of nuclei. For the same final result, the computer time is shortened by several orders of magnitude. The method can be used to study other processes in spherical and deformed nuclei, in particular, the excitation of giant resonances in reactions with different particles.[19]

4. SINGLE-PHONON STATES AND THE GIANT DIPOLE RESONANCE

Of all the giant resonances, the electric dipole resonance[34] has been studied best experimentally. Among the papers devoted to the theoretical description of the dipole resonance, those that are based on microscopic and semimicroscopic approaches have the greatest interest now. The nonphenomenological description of giant resonances permits the most complete investigation of their properties.

For deformed nuclei, the giant electric dipole resonance ($\lambda=1$) is formed by states with $K^\pi=0^-$ and 1^-. A large number of single-phonon states, whose total number reaches several hundred, participates in its formation. For example, for nuclei in the region of $A=239$ in the interval 7–20 MeV there are more than 400 phonons with $K^\pi=0^-$ and more than 1100 phonons with $K^\pi=1^-$. Essentially, the width of the resonance is the width of the region of its localization and is not related to the natural width of the individual states.

As was indicated in Sec. III, it is convenient to investigate states with intermediate and high excitation energies by means of strength functions and an averaging procedure. One can show that the averaging parameter Δ does not influence the calculated integral characteristics of resonances if

$$\Delta<\Gamma_{res}. \qquad (37)$$

The value of Δ affects only the smoothness and height of the individual peaks. If the condition (37) is satisfied, the calculated width and cross section of the resonance are determined, not by the parameter Δ, but by the properties of the single-phonon states forming the resonance. In accordance with (37), we take $\Delta\sim1$–1.5 MeV. The results of the calculations of the giant electric dipole resonance for some nuclei of the rare-earth and transuranium regions are shown in Figs. 3–6 and in Tables IV and V. Figure 3 shows the splitting of the resonance between $K=0$ and 1 because of the deformation of the nucleus. By the energies E, E_1, and E_2 in what follows we understand, respectively, the centers of gravity of the complete resonance and its projections with $K=0$ and 1. From comparison of the strength functions of the cross section of $E1$ photoabsorption calculated with $\Delta=0.1$ MeV (see Fig. 3a) and $\Delta=1.5$ MeV (see Fig. 3b), it can be seen that the region of localization of the resonance (its width) does not depend on the averaging parameter Δ.

Almost the entire strength of the resonance is concentrated in an energy interval with a width of about 10

MeV. The individual states in this interval are significantly collectivized, and the reduced probabilities of $E1$ transitions for them reach 0.1–0.5 spu. For ^{238}U, about 150 single-phonon states with $K^\pi = 0^-$ and 1^- have $B(E1, 0 \to \omega_t)$ values greater than 0.01 spu, and these states exhaust ~80% of the energy-weighted sum. Outside the region of the giant resonance, there are only very weak two-quasiparticle dipole states with $K^\pi = 0^-$ and 1^- whose $B(E1, 0 \to \omega_t)$ values are $\sim 10^{-4}$ spu and less. They can influence the radiative strength function near the neutron binding energy B_n.

It follows from Fig. 4, which is taken from Ref. 19, that the employed basis is sufficiently complete to describe the giant dipole resonance. It can also be concluded that the position of the resonance is not connected to the distribution of the density of the individual two-quasiparticle states. This indicates the importance of introducing the dipole-dipole interactions to determine the position of the resonances.

The resonances for each value of K have a complicated structure determined by shell effects. The positions of their peaks do not coincide. This leads to a splitting into two peaks of the $E1$ resonance for the majority of deformed nuclei, which is well known from the experiments. In the present calculations, the resonance with $K = 0$ has for many calculated nuclei a width that is large compared with the value usually deduced from the experiments, and therefore the low-energy peak is more weakly expressed. It can be seen from Figs. 3 and 5 that within the experimental errors there is qualitative agreement between the behavior of the theoretical and experimental photoabsorption cross sections as functions of the excitation energy. It should be noted that the splitting into two peaks is determined not only by the K splitting of the resonance, but also by the additional configuration splitting of each of them.

Calculations of the giant dipole resonances were made for even-even nuclei. However, in Fig. 5 they are in some cases compared with experimental data obtained in neighboring odd nuclei. One expects only a slight change of the giant resonances in the odd nuclei on the transition from the even-even nuclei.[35]

It can be seen from Figs. 3 and 5 that in all cases the calculations give a slight overestimation of the cross section at the maximum and are inadequate in the high-energy part (irrespective of Δ). These deviations could perhaps be partly eliminated by allowance for higher configurations.[33]

In Table IV, we give E_1, E_2, and the integrated photoabsorption cross section in the region of the giant dipole resonance, comparing them with the Thomas-Reich-Kuhn (TRK) sum rule.[31] The integration was over approximately the same energy region as in the experiments.[36-40] It can be seen that there is a completely satisfactory description of the integrated properties of the dipole resonance. A certain increase of

TABLE IV. Energies E_1 and E_2 and total photoabsorption cross sections of giant dipole resonances.

Nucleus	E_1, MeV		E_2, MeV		σ_{E_1}, b·MeV		
	exp.	theor.	exp.	theor.	exp.	theor.	TRK
^{150}Nd	12.3±0.15	13.2	16.0±0.15	15.8	2.011	1.97	2.16
^{152}Sm	12.45±0.1	13.0	15.85±0.1	15.9	2.05±0.1	2.12	2.20
^{154}Sm	12.35±0.1	13.1	16.1±0.1	15.9	2.07±0.1	2.16	2.22
^{154}Gd	11.9	13.2	15.0	16.1	2.0	2.23	2.24
^{156}Gd	11.9	13.2	15.2	16.0	2.11	2.22	2.26
	12.3	—	—	—	—	—	—
^{158}Gd	11.7	13.2	14.9	16.0	2.16	2.22	2.28
^{160}Gd	12.23	13.2	15.96	16.0	2.533	2.37	2.30
^{166}Er	12.32	12.6	15.99	15.3	—	2.32	2.41
^{168}Er	11.9	12.8	15.5	15.3	—	2.32	2.43
^{170}Yb	12.14	12.5	15.76	15.1	—	2.35	2.47
^{172}Yb	12.11	12.5	15.72	15.0	—	2.35	2.49
^{174}Yb	12.04	12.5	15.43	15.0	—	2.37	2.51
	12.3	—	15.5	—	—	—	—
^{176}Yb	12.03	12.5	15.25	14.9	—	2.34	2.53
^{176}Hf	12.36±0.04	12.8	15.71±0.06	15.2	2.571±0.012	2.45	2.55
^{178}Hf	12.41±0.05	12.3	15.75±0.06	14.8	2.58±0.015	2.40	2.57
^{180}Hf	12.41±0.04	12.2	15.75±0.05	14.7	2.535±0.012	2.39	2.59
	12.2	—	15.3	—	—	—	—
^{182}W	11.9	12.4	14.8	14.8	—	2.46	2.64
^{184}W	11.9	12.3	14.8	14.9	—	2.47	2.65
	12.5	—	15.6	—	2.65	—	—
^{186}W	12.59	12.3	14.88	14.9	3.004	2.63	2.67
	12.0	—	14.5	—	—	—	—
	12.5	—	15.2	—	2.67	—	—
^{190}Os	12.6	12.6	14.8	15.0	2.74	2.57	2.74
^{232}Th	10.99±0.16	11.7	13.9±0.13	13.3	2.92±0.32	3.04	3.30
	11.26	—	14.18	—	2.694	—	—
	11.08±0.12	—	14.07±0.14	—	2.5±0.25	—	—
^{238}U	10.97±0.13	11.1	14.25±0.18	13.2	2.95±0.29	3.06	3.39
	10.8±0.3	—	13.9±0.3	—	3.026	—	—
	10.96±0.09	—	14.04±0.13	—	2.98±0.15	—	—
	10.95±0.06	—	14.0±0.08	—	—	—	—
	10.92	—	13.98	—	—	—	—

TABLE V. Characteristics of giant dipole resonances.

Nucleus	E, MeV	Γ, MeV	Contribution to EWSR, MeV·mb	EWSR, MeV·mb	
				Model	No-model
^{150}Nd	15.4	5.2	2240	2600	2160
^{152}Sm	15.5	5.4	2310	2680	2200
^{154}Sm	15.5	5.5	2310	2680	2220
^{156}Sm	15.4	5.4	2310	2680	2240
^{154}Gd	15.6	5.6	2390	2760	2240
^{156}Gd	15.6	5.6	2380	2760	2260
^{158}Gd	15.6	5.5	2380	2760	2280
^{160}Gd	15.5	5.4	2370	2760	2300
^{156}Dy	15.7	5.8	2460	2840	2280
^{158}Dy	15.7	5.8	2460	2840	2310
^{160}Dy	15.6	5.8	2450	2840	2330
^{162}Dy	14.8	6.4	2450	2870	2350
^{164}Dy	14.8	6.4	2440	2860	2370
^{160}Er	15.0	6.6	2520	2930	2350
^{162}Er	15.0	6.5	2520	2930	2370
^{164}Er	14.9	6.5	2510	2930	2390
^{166}Er	14.9	6.5	2500	2930	2410
^{168}Er	14.8	6.4	2500	2930	2430
^{170}Er	14.8	6.3	2500	2930	2450
^{166}Yb	15.1	6.5	2600	3050	2430
^{168}Yb	15.0	6.4	2600	3040	2450
^{170}Yb	14.6	5.4	2550	3000	2470
^{172}Yb	14.6	5.4	2540	3000	2490
^{174}Yb	14.5	5.3	2530	2990	2510
^{176}Yb	14.5	5.3	2520	2990	2530
^{178}Yb	14.4	5.4	2500	2970	2550
^{170}Hf	14.8	5.1	2650	3120	2490
^{172}Hf	14.8	5.2	2650	3120	2510
^{174}Hf	14.8	5.1	2640	3120	2530
^{176}Hf	14.7	5.0	2630	3120	2550
^{178}Hf	14.2	5.8	2550	3010	2570
^{180}Hf	14.2	5.9	2530	2990	2590
^{182}W	14.3	5.6	2620	3080	2640
^{184}W	14.3	5.6	2620	3100	2650
^{186}W	14.3	5.6	2630	3110	2670
^{190}Os	14.5	5.7	2750	3270	2740
^{226}Ra	13.0	5.5	3440	4080	3220
^{228}Th	13.0	5.7	3440	4060	3270
^{230}Th	13.0	5.6	3450	4070	3290
^{232}Th	13.0	5.4	3450	4080	3300
^{230}U	12.9	5.8	3440	4040	3310
^{233}U	12.9	5.7	3450	4050	3330
^{234}U	12.9	5.6	3460	4070	3350
^{236}U	12.8	6.1	3480	4150	3370
^{238}U	12.8	6.1	3490	4170	3390
^{236}Pu	12.8	6.2	3500	4160	3390
^{238}Pu	12.8	6.1	3520	4180	3410
^{240}Pu	12.9	6.1	3520	4200	3430
^{242}Pu	12.8	6.1	3520	4200	3450
^{242}Cm	12.9	6.2	3570	4240	3480

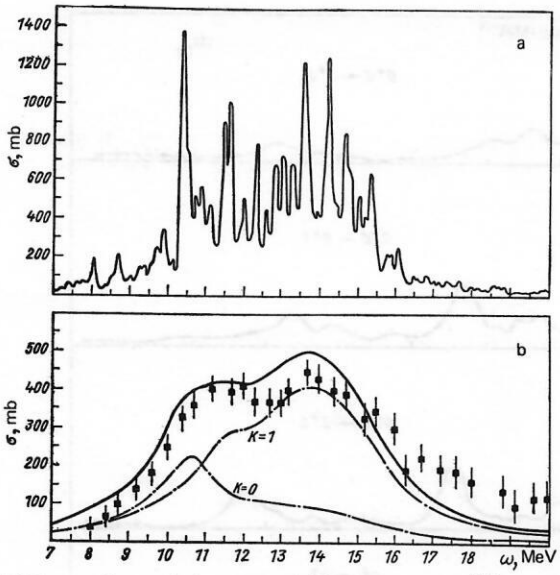

FIG. 3. Strength function of $E1$ excitation of ^{238}U. a) For $\Delta = 0.1$ MeV, b) $\Delta = 1.5$ MeV. The chain line shows resonances with $K = 0$ and 1, and the experimental data are taken from Ref. 36.

the sum rule in the experiment suggests the presence of exchange or velocity-dependent forces, which are not taken into account in the calculation of the no-model sums. In the majority of cases, the difference between the calculated and the experimental photoabsorption cross sections does not exceed 10–15%. Figure 6 shows the dependence of the position of the center of gravity of the dipole resonance and of each of the peaks $K = 0$ and 1 on A. The results of the calculations agree with the phenomenological estimates and the experimental data. In Table V, we give the results of calculations of the position and half-width $\Gamma_{1/2}$ of the giant resonance. The energy-weighted sum of the reduced probabilities of $E1$ transitions is compared with the TRK sum rule.[31]

5. SINGLE-PHONON STATES AND GIANT QUADRUPOLE RESONANCE

We consider the single-phonon space for quadrupole phonons. In the study of quadrupole phonons, i.e., phonons with $\lambda = 2$, the single-phonon states with $K^\pi = 0^+$, 1^+, and 2^+ are calculated independently. For each value of K^π, the number of single-phonon states up to excition energy 40 MeV is 2000–3000. The density of

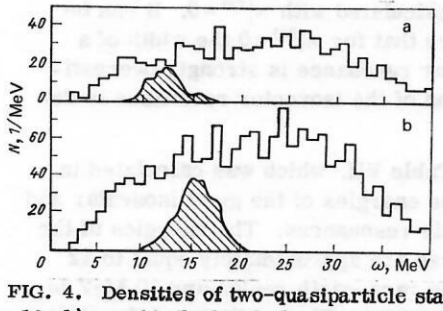

FIG. 4. Densities of two-quasiparticle states in ^{166}Er: a) $\lambda\mu = 10$, b) $\lambda\mu = 11$; the hatched regions indicate the positions of corresponding resonances in arbitrary units.

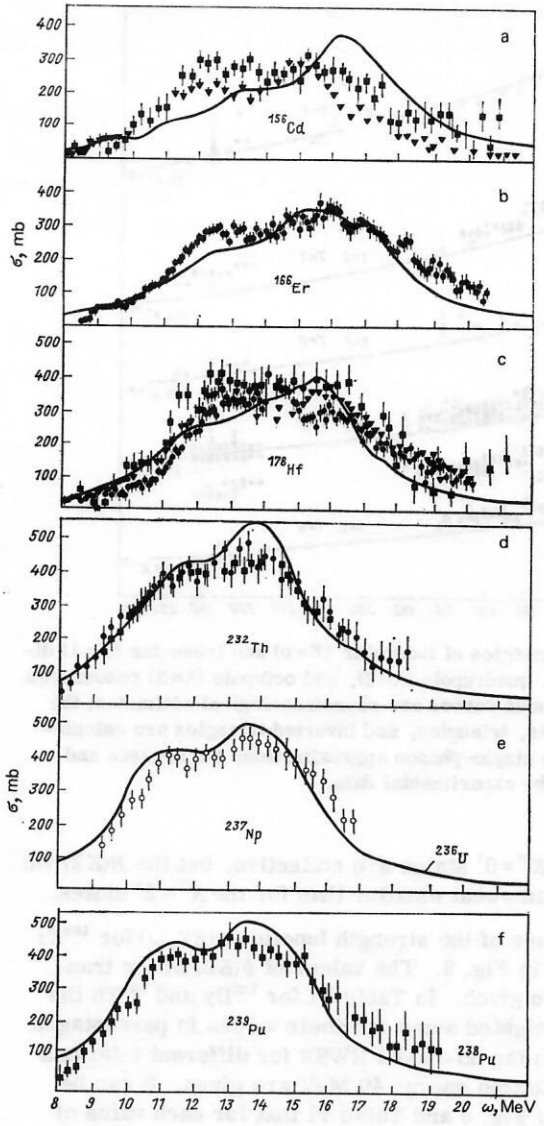

FIG. 5. Calculated and experimental cross sections of $E1$ photoabsorption.

states with $K^\pi = 2^+$ and the strength function $b(E2, \omega)$ of the reduced probability of transitions to them in ^{238}U is shown in Fig. 7. It can be seen from the figure that at excitation energy higher than 15 MeV there are ~100 solutions to the secular equation (11) in an interval of 1 MeV. Figure 7 shows that our single-particle space is sufficiently large, so that at the energy 30 MeV the density does not yet begin to fall.

We study how the strength of the single-phonon states with $K^\pi = 2^+$, 1^+, and 0^+ of even-even deformed nuclei are distributed over different intervals of excitation energy. The first $K^\pi = 2^+$ states are collective, and for them the $B(E2)$ values are equal to 2–6 single-particle units. The energies of the first states are, as a rule, lower than 1 MeV, and their contribution to the EWSR is small (of order 2%). The rotational energy of the nucleus, as a whole, is distinguished by a choice of the constant $\varkappa_0^{(21)}$ such that the energy of the lowest state with $K = 1$ is equal to zero. However, the first rotational state makes the smallest contribution to the EWSR.

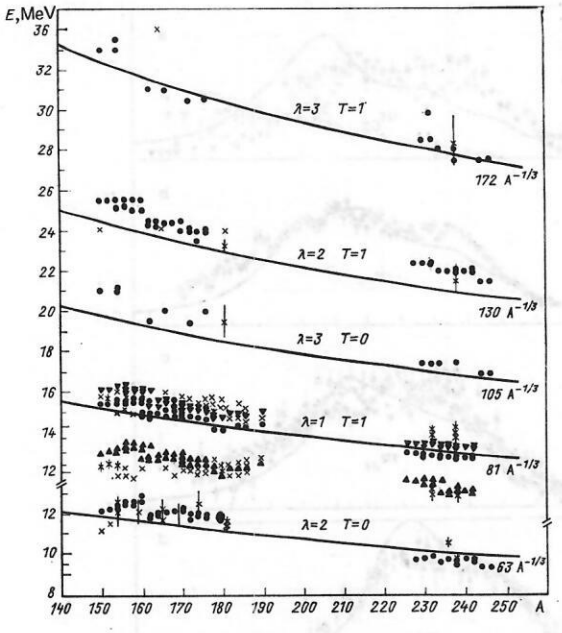

FIG. 6. Energies of isoscalar ($T=0$) and isovector ($T=1$) dipole ($\lambda=1$), quadrupole ($\lambda=2$), and octupole ($\lambda=3$) resonances. The continuous curves are phenomenological estimates; the solid circles, triangles, and inverted triangles are calculations in the single-phonon approximation; the crosses and stars are the experimental data.

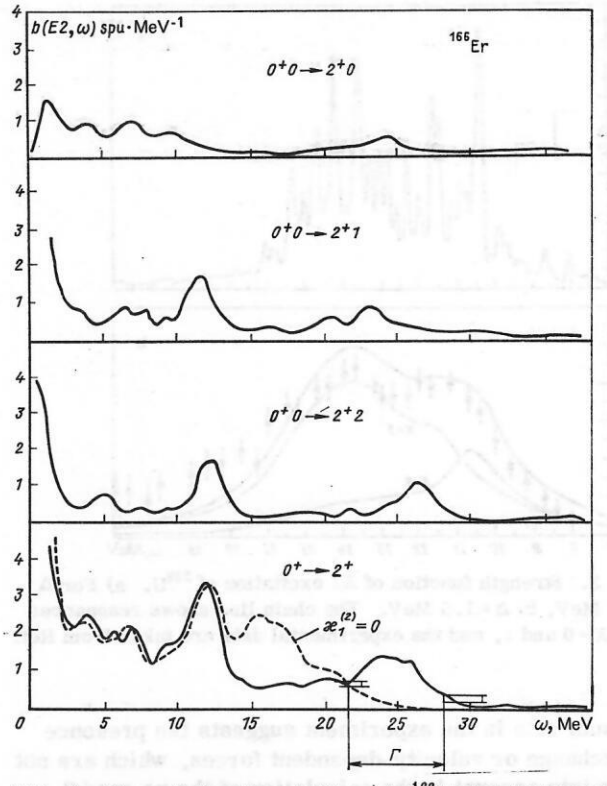

FIG. 8. Strength functions $b(E2, \omega)$ in ^{166}Er for $E2$ transitions from the ground state to states with $I^\pi K = 2^+0$, 2^+1, and 2^+2 and their total value. In the lowest figure the broken curve gives the values of $b(E2, \omega)$ calculated with $\varkappa_1^{(\lambda\mu)}=0$; Γ is the region in which the resonance is situated.

The first $K^\pi=0^+$ states are collective, but the $B(E2)$ values are somewhat smaller than for the $K^\pi=2^+$ states.

The values of the strength function $b(E2, \omega)$ for ^{166}Er are given in Fig. 8. The values of $b(E2, \omega)$ for transitions are given. In Table VI for ^{158}Dy and ^{232}Th the energy-weighted sums and their values in percentages relative to the no-model EWSR for different intervals up to excitation energy 40 MeV are given. It can be seen from Fig. 8 and Table VI that for each value of K isoscalar and isovector quadrupole resonances are clearly manifested. In the energy intervals 3–9 MeV and 14–22 MeV the values of the strength function are smaller than in the other intervals.

In deformed nuclei, the giant quadrupole resonance consists of six components with $K=0$, 1, and 2. For each value of K, the resonances have a complicated

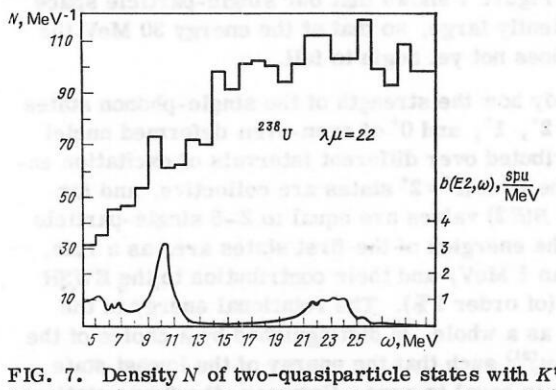

FIG. 7. Density N of two-quasiparticle states with $K^\pi=2^+$ (histogram) and the strength function $b(E2,\ 0^+_{g.s.} \to 2^+2)$ (lower curve) in ^{238}U.

shape, which is smoothed because of the large value of the parameter $\Delta=1$ MeV. The positions of the peaks of the isoscalar and isovector resonances with $K=0, 1, 2$ do not coincide. This leads to a broadening of the isoscalar and isovector resonances in the deformed nuclei compared with spherical nuclei, which agrees with the experimental data.[41] We note that there is a broadening of the giant quadrupole resonances, which are not split. The position of the isoscalar peaks with $K=0$, 1, and 2 calculated in Ref. 18 differs somewhat from the results of the calculations in Ref. 42, in which a splitting of the giant quadrupole resonance was obtained. Note that the sequence of peaks with different values of K calculated in Ref. 18 is preserved in all nuclei.

The lower part of Fig. 8 gives the total strength function $b(E2, \omega)$ for $E2$ transitions to states with $I^\pi=2^+$ with all possible K values. The dashed curve gives the values of $b(E2, \omega)$ calculated with $\varkappa_1^{(2\mu)}=0$. It can be seen from the figure that for $\varkappa_1^{(2\mu)}=0$ the width of a quadrupole isoscalar resonance is strongly overestimated. The position of the isovector resonance is determined by $\varkappa_1^{2(\mu)}$.

In Fig. 6 and in Table VII, which was calculated in Ref. 18, we give the energies of the giant isoscalar and isovector quadrupole resonances. The energies of the isoscalar resonances are approximately equal to 12 MeV in nuclei of the rare-earth region and 10 MeV in the region of the actinides. The positions of the giant isoscalar quadrupole resonances and the behavior of

TABLE VI. Calculated values of the EWSR ($\lambda=2$) in ^{158}Dy and ^{232}Th for different energy intervals.

^{158}Dy Energy interval $\Delta\omega$, MeV	EWSR, spu·MeV (model/no-model, %)				^{232}Th Energy interval $\Delta\omega$, MeV	EWSR, spu·MeV (model/no-model, %)			
	$K=0$	$K=1$	$K=2$	All K		$K=0$	$K=1$	$K=2$	All K
0—3	7(1.3)	25(4.6)	12(2.2)	44(8.1)	0—3	12(2.1)	26(4.5)	17(3.0)	55(9.6)
3—9	18(3.3)	20(3.7)	12(2.2)	50(9.2)	3—8	20(3.5)	33(5.8)	20(3.5)	73(12.8)
9—14	17(3.1)	45(8.3)	40(7.4)	102(18.8)	8—12	18(3.2)	48(8.4)	44(7.7)	110(19.2)
14—22	17(3.1)	40(7.4)	26(4.8)	83(15.3)	12—19	19(3.3)	30(5.2)	25(4.4)	74(12.9)
22—28	32(5.9)	68(12.6)	63(11.6)	163(30.1)	19—25	37(6.5)	89(15.6)	77(13.5)	203(35.5)
28—40	6(1.1)	11(2.0)	16(3.0)	33(6.1)	25—40	6(1.0)	18(3.2)	20(3.5)	44(7.7)
0—40	97(17.9)	209(38.6)	169(31.2)	475(87.6)	0—40	112(19.6)	244(42.6)	203(35.5)	559(97.7)

the strength functions $b(E2,\omega)$ below them hardly depend on $\varkappa_1^{(2\mu)}$. The results of the calculations of the energies of the resonances agree with the available experimental data (Refs. 40, 41, and 43–45).

The widths of the isoscalar and isovector giant quadrupole resonances in deformed nuclei are to a large extent determined by a certain noncoincidence of resonances with different values of K. It can be seen from Fig. 8 that the shape of the resonance differs strongly from a Gaussian curve, and one must therefore speak rather of the energy interval of localization of the resonance (total width Γ) and the energy E of its center of gravity instead of the half-width and position of the peak. To be definite, we fix the edges of this interval at the 20% level of the total height of the corresponding peak measured from the "background." In Fig. 8, these quantities are shown for the example of the isovector resonance. The results for the energies and widths determined in this manner are given in Fig. 6 and in Table VII. We emphasize that our calculated total widths Γ are virtually independent of Δ, since $\Gamma>\Delta$.

TABLE VII. Characteristics of giant quadrupole resonances.

Nucleus	$T\approx0$			$T\approx1$			EWSR	
	E, MeV	Γ, MeV	Contribution to EWSR, spu·MeV (%)	E, MeV	Γ, MeV	Contribution to EWSR, spu·MeV (%)	Model	No-Model
^{150}Nd	12.1	5	112(22)	25.5	5.5	138(27)	449	510
^{152}Sm	12.2	5	124(24)	25.5	5.5	151(29)	462	522
^{154}Sm	12.3	4,5	104(20)	25.5	5	145(29)	454	518
^{154}Gd	12.3	4,8	110(21)	25.2	5.5	157(29)	474	535
^{156}Gd	12.5	4	96(18)	25.3	5.7	163(31)	446	530
^{158}Gd	12.5	4	94(18)	25.1	6	161(31)	457	526
^{160}Gd	12.7	4	93(18)	25.1	5.8	158(30)	449	521
^{156}Dy	12.5	4,7	103(19)	25.5	5.5	161(29)	483	547
^{158}Dy	12.5	3,8	90(17)	25.5	5.5	163(30)	475	542
^{160}Dy	12.7	3,5	86(16)	25.5	7	171(32)	477	538
^{162}Dy	11.8	3,5	92(17)	24.3	6.5	177(33)	509	533
^{164}Dy	11.9	3,5	93(18)	24.3	6.2	162(31)	501	529
^{162}Er	11.8	3,7	93(17)	24.3	5.9	176(32)	527	549
^{164}Er	11.9	3	92(17)	24.3	6	177(32)	518	545
^{166}Er	12.0	3,1	97(18)	24.4	6	170(31)	510	540
^{168}Er	12.1	3,1	96(18)	24.4	6	167(31)	502	536
^{170}Er	12.1	3,1	91(17)	24.5	6	164(31)	494	532
^{170}Yb	12.2	3	93(17)	24.0	6.5	179(33)	516	547
^{172}Yb	12.0	3	96(18)	24.0	6.5	180(33)	524	543
^{174}Yb	11.8	3,5	113(21)	23.5	6.9	184(34)	515	539
^{176}Yb	11.9	3	95(18)	24.0	6.8	176(33)	508	535
^{172}Hf	11.8	3	100(18)	24.0	6.8	192(34)	550	559
^{174}Hf	11.8	3,2	105(19)	24.0	6.7	179(32)	541	554
^{176}Hf	11.8	3	99(18)	24.0	6.9	187(34)	533	550
^{228}Th	9.8	3,1	105(18)	22.4	6	215(37)	572	579
^{230}Th	9.9	3,1	104(18)	22.4	5.8	204(35)	566	575
^{232}Th	9.9	3,3	107(19)	22.3	5.9	207(36)	559	572
^{232}U	9.9	3,3	100(17)	22.3	5.4	202(35)	566	585
^{234}U	9.7	2,9	109(19)	22.0	6	214(37)	575	581
^{236}U	9.8	3	119(21)	22.0	6	216(37)	569	578
^{238}U	9.8	2,9	110(19)	22.0	6.5	212(37)	562	575
^{238}Pu	9.8	2,8	94(16)	22.0	5.7	197(34)	574	587
^{240}Pu	9.9	2,8	105(18)	22.0	6.2	208(36)	568	584
^{242}Pu	9.9	2,7	93(16)	22.0	6.7	211(36)	561	581
^{242}Cm	9.8	2,9	114(19)	22.0	6.5	210(35)	574	593
^{244}Cm	9.5	2,9	100(17)	21.5	7.3	232(39)	574	590
^{246}Cm	9.5	2,9	107(18)	21.5	7.5	233(40)	568	587

It can be seen from Table VII that the position of the giant quadrupole resonances changes very little within the regions of the rare-earth elements and the actinides. The change is even less than the changes in the energies of the first $K^\pi=2^+$ states. The variation of the energies and the $B(E\lambda)$ values for the first single-phonon states is due to the change in the chemical potential on the transition from one nucleus to another and thus to the change in the matrix elements corresponding to the first poles. In contrast, the positions of the giant resonances are determined by the matrix elements and the corresponding poles, whose contributions change little on the transition from one nucleus to another. This circumstance explains the small change in the energy of the giant quadrupole resonance with increasing A. It should be noted that the results of the calculations remain stable under a small variation of the parameters of the Woods–Saxon potential and the equilibrium deformations. The giant isoscalar and isovector resonances are manifested fairly clearly.

In Table VI we give the model EWSR for each nucleus and also the ratio of the model to the no-model EWSR values. It can be seen from this table that this ratio takes values from 0.88 to 0.99 for the case when the effective charges are zero. In Table VII, we also give the model and no-model EWSR, and it can be seen that the model EWSR values are somewhat smaller than the no-model EWSR. This indicates that the calculations of Ref. 18 take into account all the necessary part of the configuration space. Table VI gives the EWSR values for each value of K. It can be seen from the table that the contribution of all K is appreciable, and they must all be taken into account simultaneously.

6. SINGLE-PHONON STATES AND GIANT OCTUPOLE RESONANCE

We consider the single-phonon space for octupole ($\lambda=3$) phonons. There are four types of octupole phonons with $K^\pi=0^-$, 1^-, 2^-, and 3^-. The single-phonon octupole states in deformed nuclei were calculated in Ref. 8. The strength functions $b(E3,\omega)$ for $E3$ transitions to states with $I^\pi=3^-$ and $K=0$, 1, 2, and 3 in ^{238}U are shown in Fig. 9. In the lower part of the figure we have plotted the total strength function for transitions to $I^\pi=3^-$ states for $K=0,1,2,3$. In Table VIII for ^{154}Sm and ^{232}Th we give the energy-weighted sums and their fractions (in percentages) of the total no-model energy-weighted sum for different energy intervals and the

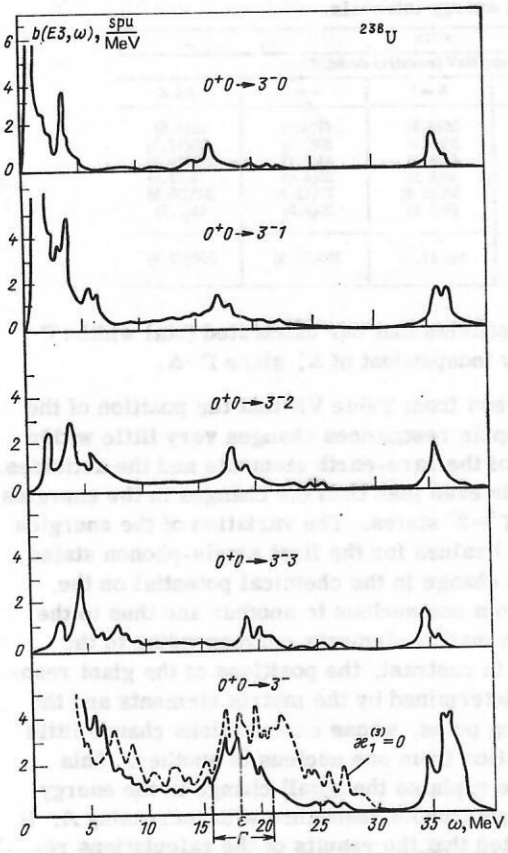

FIG. 9. Strength functions $b(E3, \omega)$ in ^{238}U for $E3$ transitions from the ground state to states with $I^\pi K = 3^-0$, 3^-1, 3^-2, and 3^-3 and their total value. In the lowest figure, the dashed curve gives the values of $b(E3, \omega)$ calculated with $\varkappa_1^{(3\mu)} = 0$; ε and Γ are the center of gravity and total width of the isoscalar resonance.

values $K = 0, 1, 2, 3$. In addition, we give the EWSR values for all K in each energy interval and the total value up to 40 MeV. The calculations were made with $\Delta = 1$ MeV, but the results depend weakly on Δ. In the calculations for ^{232}Th made with $\Delta = 0.2$ MeV appreciably smaller values are obtained in the interval 32–40 MeV and in the interval 0–2 MeV for $K = 3$. In the remaining cases, the values in Table VIII calculated with $\Delta = 1$ MeV differ from the same values calculated with $\Delta = 0.2$ MeV by not more than 10%.

The first octupole states with $K^\pi = 0^-$, 1^-, and 2^- are collective and they make a total contribution to the no-model EWSR equal to 4–5%. The extent to which these states are collective varies strongly on the transition from one nucleus to another. The first $K^\pi = 3^-$ states are weakly collective. It can be seen from Table VIII that for all values of K the behavior of the energy-weighted sums in different energy intervals is similar and the contribution of each value of K is important.

The strength function $b(E3, \omega)$ for ^{154}Sm calculated for all values of K is shown in Fig. 10. It can be asserted that there are three peaks of the giant octupole resonances: low-energy octupole resonance (LEOR), isoscalar, and isovector. The LEOR is situated at energy 2–7 MeV, and it makes a contribution to the isoscalar EWSR equal to 16–17%. The total contributions to the LEOR of particle–hole type excitations with $\Delta N = 1$ are 60% and with $\Delta N = 3$ they are 40%. The calculations of the position of the LEOR and the contributions to the EWSR are in good agreement with the experimental data.[46]

Figures 9 and 10 show the typical behavior of the octupole resonances. The isoscalar and isovector resonances are fairly clearly distinguished. In Fig. 9, the dashed curve shows the function $b(E3, \omega)$ calculated with $\varkappa_1^{(3\mu)} = 0$. Calculations with $\varkappa_1^{(3\mu)} = 0$ lead to an unphysical broadening of the giant octupole isoscalar resonance. The investigations made in Ref. 8 showed that the changes in $\varkappa_1^{(3\mu)}$ do not strongly influence the low-energy part of the strength function or the energy of the octupole isoscalar resonance. Therefore, the calculations give uniquely the position of the giant isoscalar octupole resonances in deformed nuclei at an energy of order 17–20 MeV, this value decreasing with increasing A. The position of the isoscalar resonance is determined by $\varkappa_1^{(3\mu)}$. The energies of the giant octupole resonances calculated for a number of nuclei as a function of A are given in Fig. 6. The continuous curves are the phenomenological estimates of the resonance energies.

The width of the giant octupole resonance in deformed nuclei is to a large extent determined by a certain noncoincidence of the resonances with different K values, the sequence of which is preserved in all the calculated nuclei. This is clearly demonstrated in Fig. 9. The calculated giant octupole resonances in deformed nuclei are broader than the quadrupole resonances. In discussing the width of the giant resonances, it must be borne in mind that Ref. 8 did not take into account the natural width of the levels or the interaction with higher configurations.

In the calculations, a fairly large configuration space

TABLE VIII. Calculated values of the EWSR ($\lambda = 3$) in ^{154}Sm and ^{232}Th for different energy intervals.

^{154}Sm						^{232}Th					
Energy interval $\Delta\omega$, MeV	EWSR, spu·MeV (model/no-model, %)					Energy interval $\Delta\omega$, MeV	EWSR, spu·MeV (model/no-model, %)				
	$K=0$	$K=1$	$K=2$	$K=3$	All K		$K=0$	$K=1$	$K=2$	$K=3$	All K
0—2	14(1.2)	14(1.2)	13(1.2)	7(0.6)	48(4.3)	0—2	14(1.1)	26(2.1)	18(1.5)	2(0.2)	60(4 8)
2—7	11(1.0)	32(2.9)	17(1.5)	19(1.7)	79(7.1)	2—7	16(1.3)	31(2.5)	22(1.8)	20(1.6)	89(7.2)
7—17	15(1.3)	34(3.0)	34(3.0)	21(1.9)	104(9.3)	7—15	18(1.5)	42(3.4)	28(2.3)	31(2.5)	119(9.6)
17—25	35(3.1)	70(6.2)	58(5.2)	41(3.7)	204(18.2)	15—20	32(2.6)	61(4.9)	55(4.4)	44(3.6)	192(15.5)
25—30	18(1.6)	39(3.5)	29(2.6)	21(1.9)	107(9.6)	20—25	23(1.9)	44(3.6)	34(2.8)	52(4.2)	153(12.4)
30—37	43(3.8)	80(7.2)	79(7.1)	60(5.4)	262(23.4)	25—32	57(4.6)	119(9.6)	111(9.0)	85(6.9)	372(30.1)
37—40	3(0.3)	8(0.7)	9(0.8)	14(1.2)	34(3.0)	32—40	10(0.8)	19(1.5)	21(1.7)	16(1,3)	66(5.3)
0—40	139(12.4)	277(25)	329(21.4)	183(16.4)	838(75)	0—40	170(14)	342(28)	289(23.4)	250(20)	1051(85)

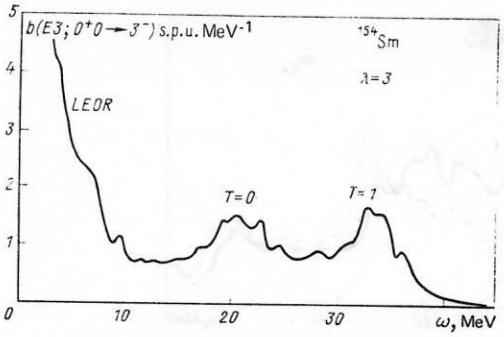

FIG. 10. Octupole resonances in ^{154}Sm.

was chosen (see Table II). As a result, the calculated value of the energy-weighted sum for the different nuclei exhausts about 80–90% of the no-model estimate of the energy-weighted sum rule (EWSR). In the region of the giant resonances, there is a large number of single-phonon states. For example, for ^{238}U in the region of the isoscalar resonance there are ~1700 and in the region of the isovector resonance ~2400 two-quasiparticle poles. The contribution to the EWSR of states with each value $K=0, 1, 2, 3$ is appreciable.

In Table IX we summarize the information on the calculations of giant octupole resonances with $\varkappa_1^{(3\mu)} = -1.5\varkappa_0^{(3\mu)}$ in deformed nuclei. For $T=0$ and 1 we give the position, total width, and energy-weighted sum of the reduced probabilities $\sum_i \omega_i B(E3, \omega_i) \approx \int \omega b(E3,\omega) d\omega$ (in brackets, its fraction measured in terms of the no-model EWSR is given).

The calculations of the giant octupole resonances agree with the available experimental data (Refs. 40 and 44–46).

7. HIGH-MULTIPOLARITY PHONONS

For the completeness of the phonon space, it is necessary to calculate single-phonon states with multipolarity $\lambda \geq 4$. In addition, there have been recent experimental indications of giant resonances of high multipolarity.[45,47] In Ref. 48, single-phonon states with $\lambda=4$, 5, 6, and 7 and the strength functions $b(E\lambda, 0^+ \to \lambda^\pi)$ in deformed nuclei were calculated.

The greatest difficulty in the calculations is due to the lack of knowledge of the constants $\varkappa_0^{(\lambda\mu)}$ and $\varkappa_1^{(\lambda\mu)}$. The values of them given by (7) and (8) are very approximate. The calculations show that an appreciable increase of the constants $\varkappa_0^{(\lambda\mu)}$ compared with the estimate (7) would contradict the experimental data, since there are no indications of the existence of low-lying collective vibrational states with $K^\pi = 4^+$, 5^-, 6^+, and 7^-. Therefore, the calculations of Ref. 48 investigated how the results are changed when $\varkappa_0^{(\lambda\mu)}$ is decreased compared with the estimate (7). Equation (8) gives a somewhat overestimated value of $\varkappa_1^{(\lambda\mu)}$, and therefore Ref. 48 studied the changes in the results of the calculations when $\varkappa_1^{(\lambda\mu)}$ is decreased compared with (8).

TABLE IX. Characteristic of giant octupole resonances.

Nucleus	$T \approx 0$			$T \approx 1$			EWBR	
	E, MeV	Γ, MeV	Contribution to EWSR, spu·MeV (%)	E, MeV	Γ, MeV	Contribution to EWSR, spu·MeV (%)	Model	No-model
^{150}Nd	21.0	8.0	230(27)	33.0	6.0	260(31)	840	1102
^{154}Sm	21.0	7.5	220(26)	33.5	6.5	300(35)	850	1119
^{154}Gd	21.0	7.5	220(26)	33.0	7.0	310(34)	880	1155
^{162}Dy	19.5	7.0	280(27)	31.0	8.0	460(45)	1030	1151
^{166}Er	20.0	7.0	280(27)	31.0	8.0	460(45)	1030	1167
^{172}Yb	19.5	6.0	220(21)	30.5	8.0	450(43)	1050	1173
^{176}Hf	20.0	6.0	220(21)	30.5	8.0	450(43)	1050	1188
^{230}Th	17.5	5.0	250(24)	28.5	7.0	440(41)	1070	1243
^{232}Th	17.5	5.0	250(24)	28.5	7.0	440(42)	1050	1236
^{234}U	17.5	5.0	270(25)	28.0	7.0	470(43)	1090	1256
^{238}U	17.5	5.0	250(23)	28.0	6.5	440(41)	1080	1242
^{244}Cm	17.0	5.0	240(22)	27.5	7.0	510(46)	1110	1274
^{246}Cm	17.0	5.0	240(22)	27.5	7.0	510(47)	1090	1268

Following the calculations of Ref. 48, we shall consider the behavior of the strength function $b(E4; 0^+ \to 4^+)$ as a function of the excitation energy ω and determine the energy regions of existence of the isoscalar and isovector $E4$ resonances. In Fig. 11 for ^{166}Er we have plotted the functions $b(E4; 0^+ \to 4^+)$, which were calculated with the value of $\varkappa_1^{(4\mu)}$ given by Eq. (8), and with three values of $\varkappa_0^{(4\mu)}$. The continuous curve was calculated with the value of $\varkappa_0^{(4\mu)}$ given by Eq. (7). It can be seen from this figure that a decrease of $\varkappa_0^{(4\mu)}$ by 17% leads to a decrease in the extent to which the states with energy lower than 15 MeV are collective. At the same time, a decrease of $\varkappa_0^{(4\mu)}$ by a further nine times leads only to a small lowering of the $b(E4; 0^+ \to 4^+)$ value. It remains an open question whether or not there are strongly collective $\lambda=4$ states with energy lower than 10 MeV. In this case, experimental study of the $E4$ transitions is very desirable.

A maximum at energies 12–18 MeV, which is shifted somewhat with decreasing $\varkappa_1^{(4\mu)}$ to higher energies, is fairly clearly manifested. Table X gives the contributions of the different energy regions to the no-model EWSR. The region 10–20 MeV makes a contribution to the EWSR of order 15%, which changes weakly when $\varkappa_0^{(4\mu)}$ varies by 10 times (13%). It can be asserted that at energy 14–18 MeV there is a giant isoscalar ($T=0$) hexadecapole resonance. There is a branch of the isoscalar resonance at energy ~30 MeV.

At excitation energy 40–50 MeV there is a giant isovector hexadecapole resonance. This region makes a contribution to the EWSR of about 39%. In the region 20–40 MeV, the $b(E4, 0^+ \to 4^+)$ values are appreciably smaller. With decreasing $\varkappa_1^{(4\mu)}$, the region in which the ($\lambda=4$, $T=1$) resonance is situated is shifted to lower excitation energies and at $\varkappa_1^{(4\mu)'} = (1/3)\varkappa_1^{(4\mu)}$ the giant iso-

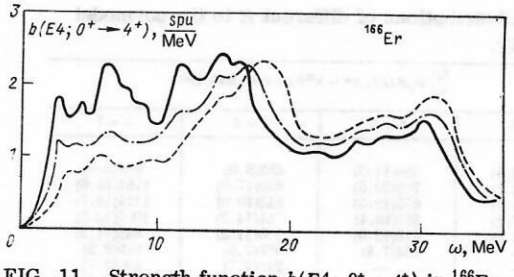

FIG. 11. Strength function $b(E4; 0^+ \to 4^+)$ in ^{166}Er calculated with $\varkappa_1^{(4)} = -2.3\times10^{-6}$ MeV·F^{-3} and the following values of $\varkappa_0^{(4)}$: 4.2×10^{-7} MeV·F^{-3} (continuous curve), 3.5×10^{-7} MeV·F^{-3} (chain curve), and 4×10^{-3} MeV·F^{-3} (broken curve).

TABLE X. Contributions S_λ to the no-model EWSR from different energy regions for resonances with $\lambda=4$, 5, 6, and 7 in ^{166}Er.

$\lambda=4$		$\lambda=5$		$\lambda=6$		$\lambda=7$	
Energy interval $\Delta\omega$, MeV	S_4, %	Energy interval $\Delta\omega$, MeV	S_5, %	Energy interval $\Delta\omega$, MeV	S_6, %	Energy interval $\Delta\omega$, MeV	S_7, %
0—10	5	0—10	5	0—10	5	0—10	5
10—18	11	10—17	6	10—20	9	10—25	15
18—32	21	17—27	13	20—37	16	25—45	15
32—40	9	27—50	24	37—50	8	45—55	5
40—50	39	50—60	37	50—65	39	55—75	39
0—50	85	0—60	85	0—65	77	0—75	79

vector hexadecapole resonance is at energy 30–40 MeV. When $|\varkappa_1^{(4\mu)}/\varkappa_0^{(4\mu)}| \gtrsim 5$, the isovector resonance is very clearly manifested.

Components with $K=0$, 1, 2, 3, and 4 contribute to the $\lambda=4$ states, and their contributions to the EWSR are not equal. This can be seen in Table XI. In the behavior of the functions $b(E4, 0^+ \to 4^+3)$ and $b(E4, 0^+ \to 4^+4)$ the maxima are situated at the same energies as in the total function $b(E4, 0^+ \to 4^+)$, but they are less clearly expressed.

Overall, one can say that, in contrast to the giant isoscalar quadrupole and octupole resonances, which are localized in fairly narrow energy intervals, the isoscalar $E4$ resonance is situated in the energy interval 10–30 MeV. The broadening of the resonance at $\lambda=4$ is explained by the contribution of the larger number of projections K and the greater number of oscillator shells, since matrix elements with $\Delta N=0, 2, 4$ contribute. The regions of greater collectivization noted above at the energies ~5, ~15, and ~30 MeV are due to a certain concentration of the states corresponding to the poles of the secular equation with energy within the oscillator shell ω_0 and energies $\sim 2\omega_0$ and $\sim 4\omega_0$.

We consider the dependence of the strength function $b(E5; 0^+ \to 5^-)$ on the excitation energy and find the region in which the resonances with $\lambda=5$ and $T=0$ and 1 are situated. It can be seen from Fig. 12, which is similar to Fig. 11 for $\lambda=4$, that at the value of $\varkappa_0^{(5\mu)}$ given by Eq. (7), and of $\varkappa_0^{(5\mu)}$ that is 22% smaller, collective states are clearly manifested at 7 MeV. They disappear if $\varkappa_0^{(5\mu)}$ is decreased by 50 times. Thus, the existence of a low-energy resonance with $\lambda=5$ appears justified.

TABLE XI. Contributions of different K to the no-model EWSR for ^{166}Er.

K	$\sum_i \omega_i B(E\lambda; 0+ \to \lambda^\pi K i)$, spu·MeV (%)			
	$\lambda=4$	$\lambda=5$	$\lambda=6$	$\lambda=7$
0	265(12.5)	380(11.0)	452(8.6)	605(8.0)
1	515(24.3)	709(20.5)	890(17.0)	1181(15.6)
2	460(21.7)	675(19.5)	842(16.0)	1111(14.7)
3	362(17.1)	567(16.4)	744(14.2)	1007(13.3)
4	243(11.5)	416(12.0)	590(11.2)	845(11.2)
5	—	254(7.4)	397(7.6)	619(8.2)
6	—	—	249(4.7)	430(5.7)
7	—	—	—	255(3.4)
	1845(87.1)	3001(86.8)	4164(79.3)	6053(80.1)

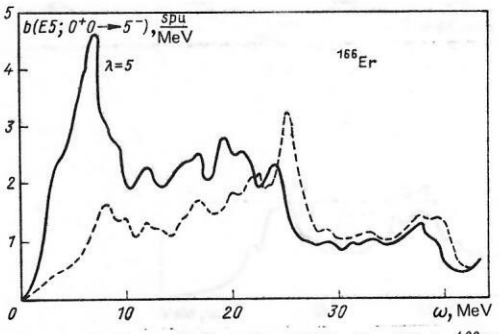

FIG. 12. Strength function $b(E5; 0^+ \to 5^-)$ in ^{166}Er calculated with $\varkappa_1^{(5)} = -6.3\times10^{-8}$ MeV·F^{-10} and the following values of $\varkappa_0^{(5)}$: 9.6×10^{-9} MeV·F^{-10} (continuous curve) and 2×10^{-10} MeV·F^{-10} (broken curve).

In the region 17–27 MeV, the function $b(E5; 0^+ \to 5^-)$ rises. With respect to the energy, it is close to $3\omega_0 \approx 22$ MeV. The contribution of this region to the EWSR is 13%. Note that with decreasing $\varkappa_0^{(5\mu)}$ the resonance with $T=0$ is manifested more clearly and becomes narrower. However, one can speak more definitely of a broad region of existence of the $E5$ resonance at energy 5–30 MeV. The regions of enhanced collectivization are situated at energies ~5, ~20, and ~35 MeV, which corresponds to a concentration of the poles of the secular equation with matrix elements for which $\Delta N=1, 3, 5$. At an excitation around 55 MeV, there is a $(\lambda=5, T=1)$ resonance. It makes a contribution to the EWSR of about 40%.

The tendency for the energy region in which the isoscalar resonances are situated to become broader with increasing λ, noted already for the resonances with $\lambda=4$ and 5, is manifested even more clearly for the resonances with $\lambda=6$ and 7. In Figs. 13 and 14 we have plotted the functions $b(E\lambda, 0^+ \to \lambda^\pi)$ for ^{166}Er with $\lambda=6$ and 7. The constants $\varkappa_0^{(\lambda\mu)}$ and $\varkappa_1^{(\lambda\mu)}$ were calculated in accordance with (7) and (8). In the same figures, we have plotted the functions $b(E\lambda, 0^+ \to \lambda^\pi)$ calculated with reduced values of $\varkappa_0^\lambda$. It can be seen from the figures that there is a broad energy region of distribution of

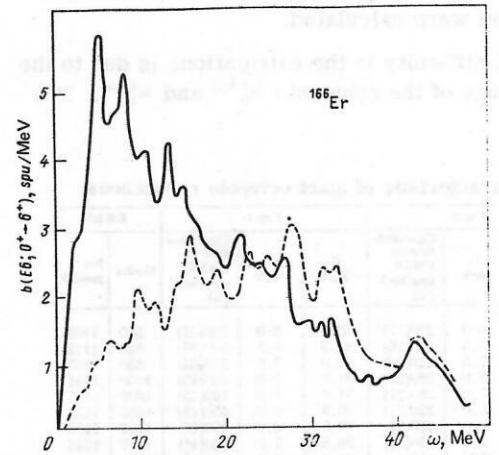

FIG. 13. Strength function $b(E6; 0^+ \to 6^+)$ in ^{166}Er calculated with $\varkappa_1^{(6)} = -1.7\times10^{-9}$ MeV·F^{-12} and the following values of $\varkappa_0^{(6)}$: 2.2×10^{-10} MeV·F^{-12} (continuous curve) and 2×10^{-11} MeV·F^{-12} (broken curve).

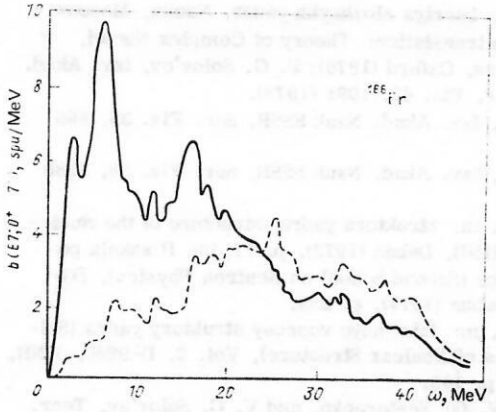

FIG. 14. Strength function $b(E7;\ 0^+ \to 7^-)$ in ^{166}Er calculated with $\varkappa_1^{(7)} = -4.3\times10^{-11}$ MeV · F^{-14} and the following values of $\varkappa_0^{(7)}$: 5×10^{-12} MeV · F^{-14} (continuous curve) and 5×10^{-13} MeV · F^{-14} (broken curve).

the giant isoscalar resonances with $\lambda = 6$ and 7. For the given multipolarities, the branches of the resonance corresponding to different ΔN are less clearly seen, and they overlap significantly. An exception is a certain separation of regions with greater degree of collectivization with energy ~42 MeV for $\lambda = 6$ and ~50 MeV for $\lambda = 7$ corresponding to $\Delta N = 6$ and 7. Of great interest is the energy region 3–15 MeV. The structure of the states in this region is very sensitive to the constant $\varkappa_0^{(\lambda\mu)}$, and experimental investigation of $E6$ and $E7$ excitations will yield a more definite conclusion concerning the existence of low-lying collective resonances with $\lambda = 6$ and 7.

At excitation energies ~60 MeV for $\lambda = 6$ and ~70 MeV for $\lambda = 7$, there are resonances with $T = 1$. Their contribution to the EWSR is about 40%. When the constant $\varkappa_1^{(\lambda\mu)}$ is decreased by three times, the energy of the resonance with $\lambda = 6$ and $T = 1$ is decreased to 50 MeV, and the isovector resonance for $\lambda = 7$ is split into two branches with energy ~45 and ~55 MeV. At the same time, there is appreciable mixing of the isoscalar and isovector resonances. The contributions of the different K to the EWSR are given in Table XI.

In Table X, for the example of ^{166}Er, we give the contributions to the no-model EWSR for $\lambda = 4$, 5, 6, and 7 for different energy intervals. It can be seen from the same table that the calculated value of the energy-weighted sum for different multipolarities exhausts 77–85% of the no-model estimate of the EWSR. This indicates that a sufficiently large configuration space was used in the calculations. More accurate allowance for the continuum will evidently influence the description of the giant isovector resonances.

The behavior of the strength functions $b(E\lambda, 0^+ \to \lambda^\pi)$ in ^{238}U as a function of the excitation energy for states with λ from 1 to 7 is shown in Fig. 15. One can very clearly see the tendency for the resonances to become broader with increasing λ and for the maxima to overlap in the region of high excitation energies. There is a possible existence of low-energy resonances with $\lambda = 5$, 6, and 7 if $\varkappa_0^{(\lambda\mu)}$ is not much smaller than the value given by (7).

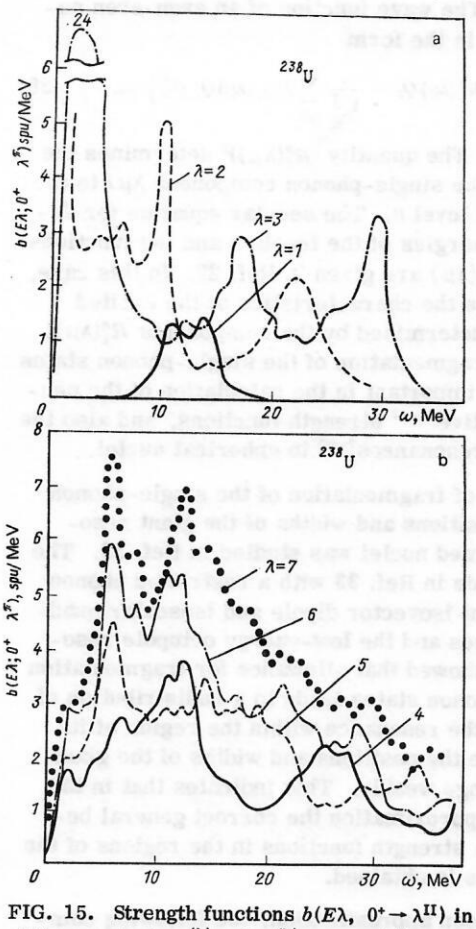

FIG. 15. Strength functions $b(E\lambda,\ 0^+ \to \lambda^{II})$ in ^{238}U. The values of the constants $\varkappa_0^{(\lambda)}$ and $\varkappa_1^{(\lambda)}$ are as follows: a) for $\lambda = 1$, 2, and 3; they are taken from Refs. 8, 18, and 19; b) for $\lambda = 4$, 5, 6, and 7, they are calculated in accordance with (7) and (8).

There must exist broad isoscalar resonances at energies 10–17 MeV for $\lambda = 4$, 10–25 MeV for $\lambda = 5$, 15–30 MeV for $\lambda = 6$, and 10–40 MeV for $\lambda = 7$. There may be a certain increase in the collectivization for $\lambda = 4$ at ~25 MeV, for $\lambda = 5$ at ~35 MeV, for $\lambda = 6$ at ~40 MeV, and for $\lambda = 7$ at ~47 MeV. The isovector resonances with $\lambda = 4$, 5, 6, and 7 are manifested fairly clearly.

CONCLUSIONS

The main aim of this paper has been to summarize the results of calculations of single-phonon states, which form the basis of the quasiparticle-phonon model of the nucleus. The description of the single-phonon states with $\lambda = 1$, 2, and 3 is unique. The calculations of the single-phonon states with $\lambda \geq 4$ contain a certain arbitrariness associated with the choice of the constants $\varkappa_0^{(\lambda\mu)}$ and $\varkappa_1^{(\lambda\mu)}$. This arbitrariness is appreciable in the description in the single-phonon approximation of giant $E\lambda$ resonances with $\lambda \geq 4$. It is not significant when the phonons with $\lambda \geq 4$ occur only in the parts of the wave function with two-phonon or quasiparticle-plus-phonon structure.

In the quasiparticle-phonon model of the nucleus, one takes into account the interactions of quasiparticles with phonons and calculates the fragmentation of single-

phonon states. The wave function of an even-even nucleus is written in the form

$$\Psi_n(K^\pi) = \Big\{ \sum_i R_i^n(\lambda\mu)\, Q_i^+ + \frac{1}{1\cdot 2} \sum_{i_1 i_2} P_{i_1 i_2}^n(\lambda\mu)\, Q_{i_1}^+ Q_{i_2}^+ \Big\} \Psi_0, \qquad (38)$$

Where $Q_i\Psi_0 = 0$. The quantity $(R_i^n(\lambda\mu))^2$ determines the contribution of the single-phonon component $\lambda\mu i$ to the wave function of level n. The secular equation for determining the energies of the levels n and the functions $R_i^n(\lambda\mu)$ and $P_{i_1 i_2}^n(\lambda\mu)$ are given in Ref. 22. In this case, one can calculate the characteristics of the excited states that are determined by the components $R_i^n(\lambda\mu)$. Allowance for fragmentation of the single-phonon states was found to be important in the calculation of the neutron[49] and radiative[14,21] strength functions, and also the widths of giant resonances[7,50] in spherical nuclei.

The influence of fragmentation of the single-phonon states on the positions and widths of the giant resonances in deformed nuclei was studied in Ref. 33. The calculations made in Ref. 33 with a restricted phonon basis of the giant isovector dipole and isoscalar quadrupole resonances and the low-energy octupole resonance in ^{154}Sm showed that allowance for fragmentation of the single-phonon states leads to a redistribution of the strength of the resonance within the region of its existence, while the positions and widths of the giant resonances change weakly. This indicates that in the single-phonon approximation the correct general behavior of the $E\lambda$ strength functions in the regions of the giant resonances is obtained.

In the quasiboson approximation, the following commutation relations are used for the phonon operators:

$$[Q_i, Q_{i'}^+] = \delta_{ii'}; \quad [Q_i, Q_{i'}] = [Q_i^+, Q_{i'}^+] = 0. \qquad (39)$$

These commutation relations are approximate, since they ignore the terms due to the fact that the phonons are constructed from fermion operators. In the single-phonon approximation, the use of the relations (39) is justified. In the construction of the two-phonon components, as in the wave function (38), or of the quasiparticle-plus-phonon components, the use of the commutation relations (39) may lead to a deterioration of the approximation. It should be emphasized that in the calculation of nuclear characteristics at low, intermediate, and high excitation energies there is no need to require fulfillment of the approximate commutation relations (39). It was shown in Refs. 22 and 51 how one can operate in the quasiparticle-phonon model with exact commutation relations for the phonon operators. Allowance for the exact commutation relations means that one takes into account the fact that the phonons are constructed from fermions and the Pauli principle is satisfied exactly. It was shown in Ref. 51 that allowance for the exact commutation relations between the phonon operators in the calculations with a wave function in the form (38) leads to a more complicated secular equation and a shift of the two-phonon poles.

Thus, in calculations in the quasiparticle-phonon model of the nucleus, in which the Pauli principle is taken into account exactly, one can again use the space of single-phonon states as a basis.

[1] V. G. Solov'ev, Teoriya slozhnykh yader, Nauka, Moscow (1971); English translation: Theory of Complex Nuclei, Pergamon Press, Oxford (1976); V. G. Solov'ev, Izv. Akad. Nauk SSSR, Ser. Fiz. **42**, 1991 (1978).
[2] V. G. Solov'ev, Izv. Akad. Nauk SSSR, Ser. Fiz. **35**, 666 (1971).
[3] V. G. Solov'ev, Izv. Akad. Nauk SSSR, Ser. Fiz. **38**, 1580 (1974).
[4] V. G. Solov'ev, in: Struktura yadra (Structure of the Nucleus), D-6465, JINR, Dubna (1972), p. 77; in: II shkola po neĭtronnoĭ fizike (Second School on Neutron Physics), D3-7991, JINR, Dubna (1974), p. 233.
[5] V. G. Solov'ev, in: Izbrannye voprosy struktury yadra (Selected Problems of Nculear Structure), Vol. 2, D-9920, JINR, Dubna (1976), p. 146.
[6] L. A. Malov, V. O. Nesterenko, and V. G. Solov'ev, Teor. Mat. Fiz. **32**, 134 (1977).
[7] V. G. Soloviev, Ch. Stoyanov, and A. I. Vdovin, Nucl. Phys. **A288**, 376 (1977).
[8] L. A. Malov, V. O. Nesterenko, and V. G. Soloviev, J. Phys. G: Nucl. Phys. **3**, L219 (1977); Phys. Lett. **B64**, 247 (1976).
[9] L. A. Malov and V. G. Solov'ev, Yad. Fiz. **21**, 502 (1975) [Sov. J. Nucl. Phys. **21**, 263 (1975)]; Teor. Mat. Fiz. **25**, 265 (1975).
[10] L. A. Malov and V. O. Nesterenko, Soobshchenie (Communication), R4-8206 [in Russian], JINR, Dubna (1974); S. V. Akulinichev and L. A. Malov, Soobshchenie (Communication), R4-8844 [in Russian], JINR, Dubna (1974).
[11] L. A. Malov and V. G. Soloviev, Nucl. Phys. **A270**, 87 (1976).
[12] L. A. Malov and V. G. Solov'ev, Yad. Fiz. **26**, 729 (1977) [Sov. J. Nucl. Phys. **26**, 384 (1977)].
[13] L. A. Malov and V. G. Solov'ev, Yad. Fiz. **23**, 53 (1976) [Sov. J. Nucl. Phys. **23**, 27 (1976)].
[14] Chan Zuy Khoung, V. G. Soloviev, and V. V. Voronov, J. Phys. G: Nucl. Phys. **5**, L79 (1979); V. V. Voronov, V. G. Solov'ev, and Ch. Stoyanov. Pis'ma Zh. Eksp. Teor. Fiz. **25**, 459 (1977) [JETP Lett. **25**, 430 (1977)].
[15] V. G. Soloviev, Neutron Capture Gamma-Ray Spectroscopy, Petten, Reactor Centrum. Nederland (1975), p. 99.
[16] V. G. Solov'ev, in: Neĭtronnaya fizika. Materialy III konferentsii po neĭtronnoĭ fizike (Neutron Physics. Proc. Third Conference on Neutron Physics), Part 3, Moscow (1976), p. 53.
[17] D. Dambasuren *et al.*, J. Phys. G: Nucl. Phys. **2**, 25 (1976).
[18] G. Kyrchev, L. A. Malov, V. O. Nesterenko, and V. G. Solov'ev, Yad. Fiz. **25**, 951 (1977) [Sov. J. Nucl. Phys. **25**, 506 (1977)].
[19] S. V. Akulinichev and L. A. Malov, J. Phys. G: Nucl. Phys. **3**, 625 (1977); S. V. Akulinichev and V. M. Shilov, J. Phys. G: Nucl. Phys. **3**, L213 (1977); S. V. Akulinichev and V. M. Shilov, Yad. Fiz. **27**, 670 (1978) [Sov. J. Nucl. Phys. **27**, 358 (1978)].
[20] V. G. Soloviev, in: Proc. Intern. Conf. on the Interactions of Neutrons with Nuclei, Vol. 1, Univ. of Lowell, Lowell, Mass. (1976), p. 421.
[21] V. G. Soloviev, Ch. Stoyanov, and V. V. Voronov, Nucl. Phys. **A304**, 503 (1978); V. Yu. Ponomarev *et al.*, Nucl. Phys. **323**, 446 (1979).
[22] V. G. Solov'ev, Fiz. Elem. Chastits At. Yadra **9**, 860 (1978) [Sov. J. Part. Nucl. **9**, 343 (1978)].
[23] A. I. Vdovin *et al.*, Fiz. Elem. Chastits At. Yadra **7**, 952 (1976) [Sov. J. Part. Nucl. **7**, 380 (1976)].
[24] B. N. Kalinkin, Ya. Grabovski, and F. A. Gareev, Acta Phys. Pol. **30**, 999 (1966); F. A. Gareev, S. P. Ivanova, and B. N. Kalinkin, Acta Phys. Pol. **30**, 461 (1966); F. A. Gareev, S. P. Ivanova, and B. N. Kalinkin, Izv. Akad. Nauk SSSR, Ser. Fiz. **33**, 1690 (1968).
[25] V. M. Strutinskiĭ, Yad. Fiz. **3**, 614 (1966) [Sov. J. Nucl.

Phys. 3, 449 (1966)]; Nucl. Phys. **A95**, 420 (1976).
[26]F. A. Gareev *et al.*, Fiz. Elem. Chastits At. Yadra **4**, 357 (1973) [Sov. J. Part. Nucl. **4**, 148 (1973)].
[27]F. A. Gareev *et al.*, Nucl. Phys. **A171**, 134 (1971).
[28]A. Bohr and B. Mottelson, Nuclear Structure, Vols. 1 and 2, Benjamin (1969, 1975) (Russian translation published by Mir, Moscow: Vol. 1 in 1971 and Vol. 2 in 1974).
[29]E. P. Grigor'ev and V. G. Solov'ev, Struktura chetnykh deformirovannykh yader (Structure of Even Deformed Nuclei), Nauka (1974).
[30]S. P. Ivanova, L. A. Komov, L. A. Malov, and V. G. Solov'ev, Fiz. Elem. Chastits At. Yadra **7**, 450 (1976) [Sov. J. Part. Nucl. **7**, 175 (1976)].
[31]D. R. Bes, R. A. Broglia, and B. S. Nilsson, Phys. Rep. **C16**, 1 (1975).
[32]O. Nathan and S. G. Nilsson, in: Alpha-, Beta-, and Gamma-Ray Spectroscopy, Vol. 2 (ed. K. Siegbahn), North-Holland, Amsterdam (1965), p. 601 (Russian translation published by Atomizdat, Moscow (1969)).
[33]G. Kyrchev and L. A. Malov, Izv. Akad. Nauk SSSR, Ser. Fiz. **43**, 107 (1979).
[34]B. L. Berman and S. C. Fultz, Rev. Mod. Phys. **47**, 713 (1975).
[35]M. Danos, W. Greiner, and C. B. Kohr, Phys. Rev. B **138**, 1055 (1965); S. V. Akulinichev and L. A. Malov, Preprint E4-9758, JINR, Dubna (1976).
[36]G. M. Gurevich, L. E. Lazareva, V. M. Mazur, and G. V. Solodukhov, Pis'ma Zh. Eksp. Teor. Fiz. **23**, 411 (1976) [JETP Lett. **23**, 370 (1976)]; G. M. Gurevich *et al.*, Nucl. Phys. **A273**, 326 (1976); G. M. Gurevich *et al.*, Pis'ma Zh. Eksp. Teor. Fiz. **28**, 168 (1978) [JETP Lett. **28**, 157 (1978)].
[37]O. V. Vasil'ev, V. A. Semenov, and S. F. Semenko, Yad. Fiz. **13**, 463 (1971) [Sov. J. Nucl. Phys. **13**, 259 (1971)]; A. M. Goryachev, G. N. Zalessnyĭ, S. F. Semenko, and B. A. Tulupov, Yad. Fiz. **17**, 463 (1973) [Sov. J. Nucl. Phys. **17**, 236 (1973)]; A. M. Goryachev and G. N. Zalessnyĭ, in: Voprosy teoreticheskoĭ i yadernoĭ fiziki (Problems in Theoretical and Nuclear Physics), No. 5, Izd. Saratovskogo Univ. (1976), p. 42.
[38]B. I. Goryachev *et al.*, Yad. Fiz. **23**, 1145 (1976) [Sov. J. Nucl. Phys. **23**, 609 (1976)].
[39]A. Veyssiere *et al.*, Nucl. Phys. **A199**, 45 (1973); P. Carlos *et al.*, Nucl. Phys. **A225**, 171 (1974); T. Bar-Noy and R. Morch, Nucl. Phys. **A229**, 417 (1974).
[40]W. A. Houk *et al.*, Preprint, Naval Postgraduate School, Monterey, CA; USA (1977).
[41]A. Schwierczinski *et al.*, Phys. Lett. **B55**, 171 (1975); N. Marty *et al.*, Nucl. Phys. **A238**, 93 (1975); T. Kishmoto *et al.*, Phys. Rev. Lett. **35**, 552 (1975); D. Y. Horen, F. E. Bertrand, and M. B. Lewis, Phys. Rev. **9**, 1607 (1974); J. M. Moss *et al.*, Phys. Lett. **B53**, 51 (1974); G. R. Satchler, Phys. Rep. **C14**, 97 (1974).
[42]D. Zawischa and J. Speth, Phys. Rev. Lett. **36**, 843 (1976); D. Zawischa, J. Speth, and D. Pal, Nucl. Phys. **A311**, 445 (1978).
[43]F. E. Bertrand, Ann. Rev. Nucl. Sci. **26**, 457 (1976); D. J. Horen *et al.*, Phys. Rev. C **11**, 1247 (1975); J. D. T. Arruda Neto *et al.*, Phys. Rev. C **18**, 867 (1978); J. D. T. Arruda Neto *et al.*, Preprint IFUSP/P-154, 1978, Inst. Univ. Sao Paulo; H. Miura and Y. Torizuka, Phys. Rev. C **16**, 1688 (1977); D. H. Youngblood *et al.*, Phys. Rev. C **13**, 994 (1976).
[44]G. L. Moore *et al.*, Z. Naturforsch. **31a**, 668 (1976).
[45]R. S. Hicks *et al.*, Nucl. Phys. **A278**, 261 (1977); R. Pitthan, Nucleonika **24**, 449 (1979).
[46]J. M. Moss *et al.*, Phys. Rev. Lett. **37**, 816 (1976).
[47]N. V. Geramb and K. Amos, Lett. Nuovo Cimento **14**, 526 (1975); A. Goswami and L. Lin, Phys. Lett. **B42**, 310 (1972); R. D. Bagnell *et al.*, Phys. Lett. **B66**, 129 (1977); A. A. Nemashkalo *et al.*, Pis'ma Zh. Eksp. Teor. Fiz. **26**, 569 (1977) [JETP Lett. **26**, 422 (1977)].
[48]M. A. Kiselev, L. A. Malov, V. O. Nesterenko, and V. G. Solov'ev, Izv. Akad. Nauk SSSR, Ser. Fiz. **42**, 1842 (1978).
[49]V. V. Voronov, V. G. Solov'ev, and O. Stoyanova, Preprint E4-12500, JINR, Dubna (1979).
[50]A. I. Vdovin, Ch. Stoyanov, and I. P. Yudin, Preprint R4-11108 [in Russian], JINR, Dubna (1977); V. G. Soloviev, Ch. Stoyanov, and V. V. Voronov, Phys. Lett. **B79**, 187 (1978); V. Yu. Ponomarev *et al.*, Preprint E4-12093, JINR, Dubna (1979).
[51]R. V. Dzholos, Kh. L. Molina, and V. G. Solov'ev, Teor. Mat. Fiz. **40**, 245 (1979).

Translated by Julian B. Barbour